

A kiwellin disarms the metabolic activity of a secreted fungal virulence factor

Xiaowei Han¹, Florian Altegoer², Wieland Steinchen², Lynn Binnebesel², Jan Schuhmacher^{2,6}, Timo Glatzer³, Pietro I. Giammarinaro², Armin Djamei^{1,7}, Stefan A. Rensing^{4,5}, Stefanie Reissmann¹, Regine Kahmann^{1*} & Gert Bange^{2*}

Fungi-induced plant diseases affect global food security and plant ecology. The biotrophic fungus *Ustilago maydis* causes smut disease in maize (*Zea mays*) plants by secreting numerous virulence effectors that reprogram plant metabolism and immune responses^{1,2}. The secreted fungal chorismate mutase Cmu1 presumably affects biosynthesis of the plant immune signal salicylic acid by channelling chorismate into the phenylpropanoid pathway³. Here we show that one of the 20 maize-encoded kiwellins (*ZmKWL1*) specifically blocks the catalytic activity of Cmu1. *ZmKWL1* hinders substrate access to the active site of Cmu1 through intimate interactions involving structural features that are specific to fungal Cmu1 orthologues. Phylogenetic analysis suggests that plant kiwellins have a versatile scaffold that can specifically counteract pathogen effectors such as Cmu1. We reveal the biological activity of a member of the kiwellin family, a widely conserved group of proteins that have previously been recognized only as important human allergens.

Maize smut disease is caused by the biotrophic fungus *U. maydis*^{1,2}. To induce plant tumours, *U. maydis* establishes an extended interaction zone between fungal hyphae and the invaginated plant plasma membrane, into which it secretes an abundance of effector proteins that reprogram host metabolism and interfere with plant defence responses. The secreted chorismate mutase Cmu1 is specifically upregulated during colonization of the plant and is among the most highly expressed fungal genes during biotrophic development³. Cmu1 belongs to the AroQ-class of chorismate mutases and has been shown to catalyse branch-point reactions within the biosynthesis of phenylalanine and tyrosine, in which prephenate is generated from chorismate³. During colonization Cmu1 is translocated to the cytosol of plant cells, where its chorismate mutase activity seems to channel chorismate into the phenylpropanoid pathway, thereby preventing the biosynthesis of salicylic acid³, a central signal for plant innate immune responses against biotrophic pathogens (reviewed in ref. ⁴). Interfering with salicylic acid biosynthesis pathways is a general strategy of plant-pathogenic fungi, oomycetes and nematodes, and is used by secreted chorismate mutase and isochorismatase enzymes^{5–7}.

To elucidate the characteristics of the Cmu1 enzyme, we determined its crystal structure at a resolution of 1.9 Å (Fig. 1a, Extended Data Table 1). Like the prototypical chorismate mutase Aro7p of *Saccharomyces cerevisiae*⁸, Cmu1 forms a homodimer, in which each monomer harbours nine α -helices and identical active sites (Fig. 1b, Extended Data Fig. 1). However, Cmu1 differs from Aro7p and the housekeeping maize chorismate mutases *ZmCM1* and *ZmCM2* (Extended Data Fig. 2, Extended Data Table 1) in a region that is critical for the allosteric regulation of Aro7p by tryptophan and tyrosine (that is, activation and repression, respectively)⁹. In Aro7p, *ZmCM1* and *ZmCM2*, helix α 2 and an adjacent loop region establish the binding site for the regulatory amino acids tryptophan and tyrosine (Fig. 1c, left; Extended Data Fig. 2d). In Cmu1, however, an additional α -helix

(α 2a) and an extensive loop region (ELR) follow helix α 2 and wrap around Cmu1 (Fig. 1c, right). These differences could explain the absence of allosteric regulation of Cmu1 by tryptophan and tyrosine³. We therefore reinvestigated the effect of tryptophan and tyrosine on the chorismate mutase activities of Cmu1 and Aro7p. Whereas the activity of Aro7p was at least ten times greater in the presence of tryptophan, no change in the activity of Cmu1 was observed (Fig. 1d). In the presence of tyrosine, Aro7p activity was decreased, whereas Cmu1 activity was unaltered (Fig. 1d). This shows that Cmu1 is not allosterically regulated by the amino acids tryptophan and tyrosine, and can therefore be considered as resistant to fluctuations in amino acid levels in the cytosol of maize. These observations raise the question of whether plants have developed strategies to hinder the activity of this pathogen enzyme in order to control the infection process.

To identify potential host factors affecting Cmu1 activity, maize seedlings were infected with a *U. maydis* strain expressing a triple haemagglutinin (HA)-tagged Cmu1 driven by its native promoter. Co-immunoprecipitation (co-IP) followed by liquid chromatography–mass spectrometry unambiguously identified a hypothetical maize protein (annotation: GRMZM2G073114) with considerable amino acid sequence identity to the kiwellin protein (KWL1) from the kiwi plant (Extended Data Fig. 3a). Therefore, we termed the hypothetical maize protein *ZmKWL1*. Notably, recent RNA sequencing analysis of fungal and plant genes during the biotrophic stage of *U. maydis* shows that *ZmKWL1* is the only one of the 20 kiwellin genes that is strongly induced upon infection¹⁰ (Extended Data Fig. 3b). To specify the role of *ZmKWL1* during *U. maydis* infection, the Foxtail mosaic virus (FoMV)-based gene silencing (VIGS) system was used¹¹. To silence *ZmKWL1* in maize, the *ZmKWL1* VIGS construct (pFoMV-*ZmKWL1*^{181–480}) was first amplified after biolistic transformation of maize and the sap of virus-producing plants was then used for rub-inoculation of maize seedlings. Silencing efficiency was tested by quantitative PCR (qPCR) six days after virus infection. *ZmKWL1* transcripts were significantly reduced in leaves from pFoMV-*ZmKWL1*^{181–480} VIGS plants in comparison to those from pFoMV-V infected control plants that had received the empty vector (Extended Data Fig. 3c). Next we challenged VIGS and control plants with the *U. maydis* solopathogenic strain CL13¹² to determine whether silencing of *ZmKWL1* could alter disease development. CL13 is a weak pathogen because it lacks autocrine pheromone stimulation¹³. In contrast to plants infected by pFoMV-V, plants infected by pFoMV-*ZmKWL1*^{181–480} that expressed the silencing construct showed a significant increase in susceptibility to CL13 infection (Fig. 1e, Extended Data Fig. 3d). This suggests that *ZmKWL1* is a defence protein that protects maize from infection by *U. maydis*.

The Cmu1–*ZmKWL1* interaction was further substantiated by pull-down assays using hexahistidine (His₆)-tagged *ZmKWL1* expressed in *Nicotiana benthamiana* and HA₃-tagged Cmu1 expressed in the supernatant of an *U. maydis* culture. After pull-down with Ni-NTA agarose,

¹Department of Organismic Interactions, Max Planck Institute for Terrestrial Microbiology, Marburg, Germany. ²Philipps-University Marburg, Center for Synthetic Microbiology (SYNMIKRO) and Department of Chemistry, Marburg, Germany. ³Facility for Mass Spectrometry and Proteomics, Max Planck Institute for Terrestrial Microbiology, Marburg, Germany. ⁴Faculty of Biology, Philipps-University, Marburg, Germany. ⁵BIOSS Centre for Biological Signalling Studies, University of Freiburg, Freiburg, Germany. ⁶Present address: Max Planck Institute of Molecular Cell Biology and Genetics, Dresden, Germany. ⁷Present address: Gregor Mendel Institute (GMI), Austrian Academy of Sciences, Vienna Biocenter (VBC), Vienna, Austria. *e-mail: kahmann@mpi-marburg.mpg.de; gert.bange@synmikro.uni-marburg.de

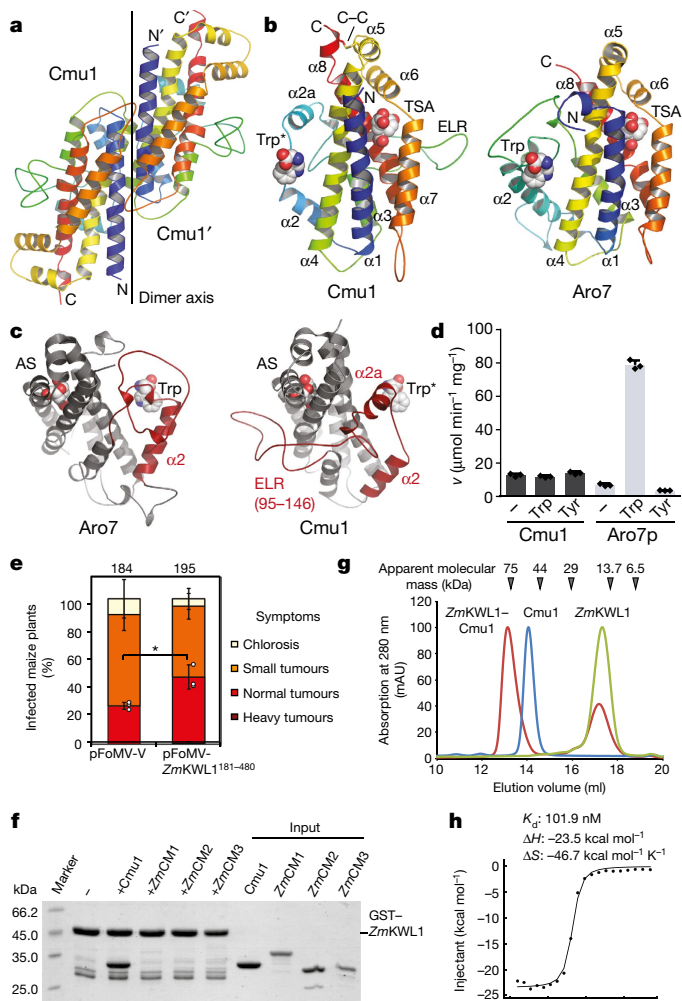


Fig. 1 | Chorismate mutase Cmu1. **a**, Cartoon representation of the Cmu1 homodimer. Each monomer is rainbow-coloured from the N- to the C terminus. **b**, Side-by-side view of the superimposed monomers of Cmu1 (left; this study) and Aro7p (right; PDB: 3CSM⁹). Aro7p is in complex with an *endo*-oxabicyclic transition state analogue inhibitor (TSA) and tryptophan bound to the active and allosteric sites, respectively. A tryptophan (asterisk) was placed into the structure of the Cmu1 monomer to indicate the position equivalent to that in Aro7p. **c**, Cmu1 and Aro7p differ in the region (red) required for the allosteric regulation of Aro7p by tryptophan and tyrosine. AS, active site. **d**, Activity of Cmu1 and Aro7p (mean \pm s.d. of $n = 3$ technical replicates) in the absence and the presence of 10 μ M of tryptophan or 50 μ M of tyrosine. **e**, Six-day-old maize seedlings were rub-inoculated with viral sap containing pFoMV-V or pFoMV-ZmKWL1¹⁸¹⁻⁴⁸⁰. Rub-inoculated seedlings were infected with CL13 six days after viral inoculation. Disease symptoms were scored 12 days post CL13 infection. Data represent mean of $n = 3$ biologically independent experiments. Total numbers of infected plants are indicated above the respective columns. P value was determined by unpaired two-sided Student's t -test. * $P = 0.0184$. **f**, Coomassie-stained SDS-PAGE of an *in vitro* interaction assay using glutathione *S*-transferase (GST)-tagged ZmKWL1, Cmu1, and the three chorismate mutases of maize: ZmCM2, which localizes in the cytosol³; ZmCM1, which localizes in the chloroplast; and ZmCM3, which is predicted to be secreted. Input controls are on the right as indicated. **g**, Size-exclusion chromatography of ZmKWL1 (green), Cmu1 (blue) and Cmu1-ZmKWL1 (red). **h**, Isothermal titration calorimetry analysis of Cmu1 and ZmKWL1, yielding a K_d value of 101.9 nM. In **f-h**, experiments were repeated independently twice with similar results and representative experiments are shown.

ZmKWL1 but not the empty vector control clearly immunoprecipitated Cmu1 (Extended Data Fig. 3e). Moreover, purified ZmKWL1 interacted with purified Cmu1 in an *in vitro* pull-down assay; however, it

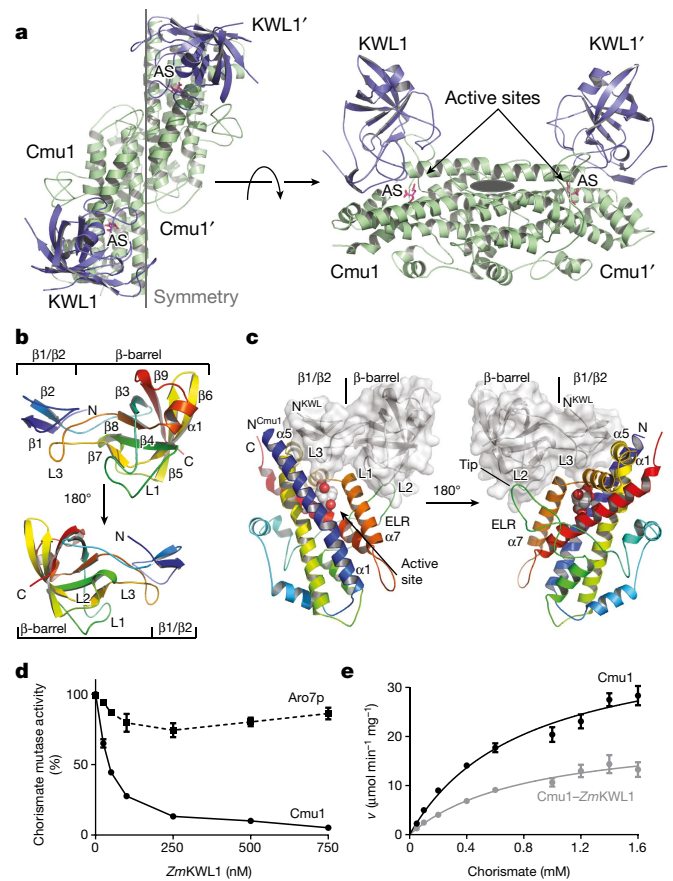


Fig. 2 | The Cmu1-ZmKWL1 complex. **a**, Cartoon representation of the complex of Cmu1 (green) and ZmKWL1 (blue). Citrate (red) from the crystallization buffer was found in the active site. **b**, ZmKWL1 consists of a central β -barrel domain and an anti-parallel β -sheet comprising $\beta 1$ and $\beta 2$ at its N terminus. The loops L1, L2 and L3 are crucial for the interaction of ZmKWL1 with Cmu1. **c**, ZmKWL1 (grey and transparent) blocks entry of the substrate into the active site of Cmu1 (rainbow cartoon). The active site of Cmu1 containing citrate as the substrate mimic is shown as spheres. **d**, Chorismate mutase activity of Cmu1 (solid line) and Aro7p (dashed line) in the presence of increasing concentrations of ZmKWL1. Chorismate mutase activity in the absence of ZmKWL1 was set to 100%. **e**, A plot of velocity against substrate concentration for Cmu1 activity in the absence (black) and presence (grey) of stoichiometric amounts of ZmKWL1. In **d**, **e**, data represent mean \pm s.d. of $n = 3$ technical replicates.

did not interact with the three purified chorismate mutases of maize (Fig. 1f). Size-exclusion chromatography shows that purified Cmu1 and ZmKWL1 alone migrated at apparent molecular masses that correspond to the homodimer and the monomer, respectively (Fig. 1g). When mixed, Cmu1 and ZmKWL1 co-migrated in a homogenous peak, the molecular mass of which is best explained by two molecules of Cmu1 and two molecules of ZmKWL1. Analysis by isothermal titration calorimetry gave a dissociation constant (K_d) of approximately 100 nM for the Cmu1-ZmKWL1 interaction (Fig. 1h). Together, these data show that two molecules of ZmKWL1 strongly interact with one Cmu1 homodimer.

Next, we determined the crystal structure of the Cmu1-ZmKWL1 complex at a resolution of 1.8 Å (Extended Data Table 1). The structure shows that two ZmKWL1 bind in a highly symmetric manner to one Cmu1 homodimer (Fig. 2a). The Cmu1-ZmKWL1 interaction is mainly established through a mixed interface of polar and non-polar interactions and accounts for approximately 1,200 Å² of buried surface area. The two ZmKWL1 molecules localize in close proximity to the two active sites present within the Cmu1 homodimer. ZmKWL1 consists of nine β -strands (named $\beta 1$ to $\beta 9$) and one short α -helical segment connecting $\beta 8$ and $\beta 9$ (Fig. 2b). The β -strands $\beta 3$ to $\beta 9$ form a

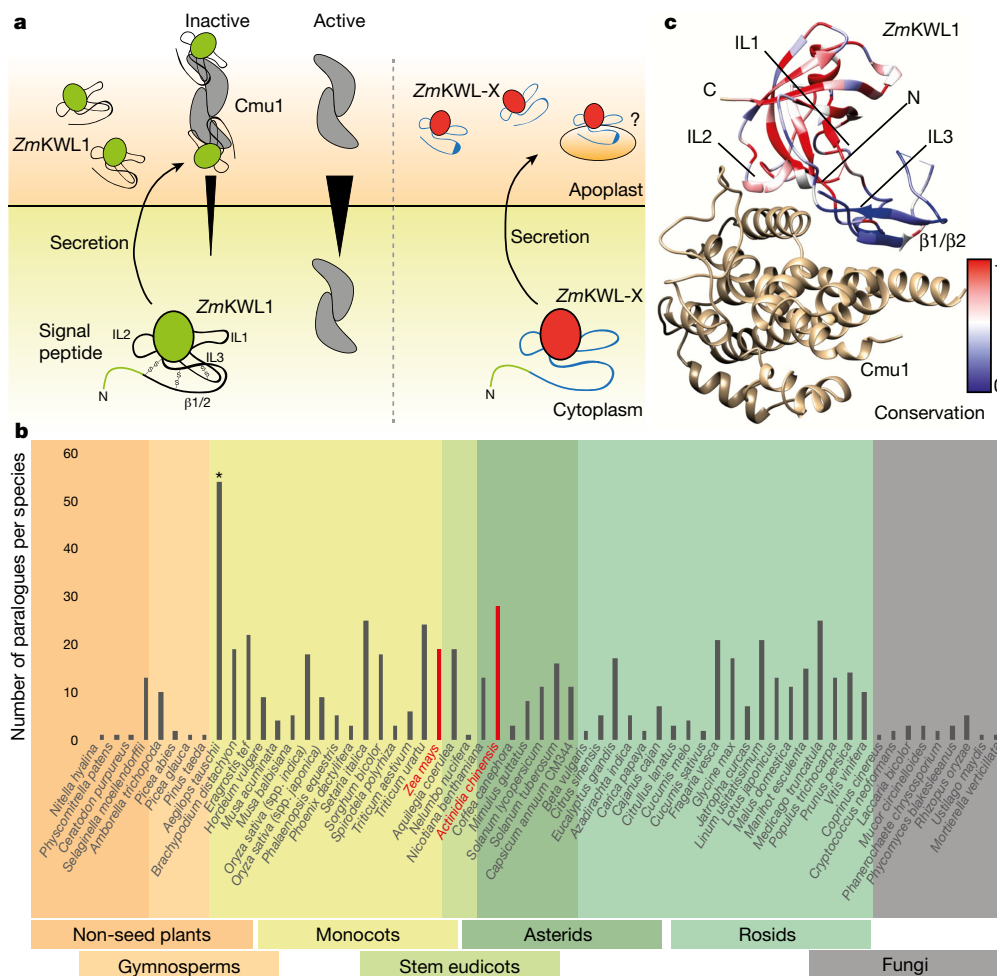


Fig. 3 | Kiwellins are a highly versatile class of defence proteins. a, Schematic of the mechanism of action of kiwellin. *ZmKWL1* is produced in the plant cell and probably secreted to the apoplast via its N-terminal signal sequence. In the apoplastic space, *ZmKWL1* binds *Cmu1* and disarms its activity; binding may also decrease the import of *Cmu1* into the cytoplasm. Further kiwellin homologues (*ZmKWL-X*) might be produced by the plant cell and secreted, but their cognate targets are

unknown (right). **b**, The number of kiwellin paralogue genes per plant species, colour-coded according to taxonomic group. All but six of the analysed plant genomes contained more than one kiwellin paralogue (average 11, median 10, highest number found 54). Notably, several fungal genomes also contain kiwellin-encoding genes. **c**, Amino acid conservation between the 19 kiwellins from *Z. mays* mapped onto the structure of *ZmKWL1*. Red and blue denote highly conserved and non-conserved regions, respectively.

β -barrel, which is stabilized by three disulfide bridges (Cys64–Cys157, Cys104–Cys129 and Cys151–Cys167). At the N-terminal end of the barrel, $\beta 1$ and $\beta 2$ form anti-parallel β -strands that are stabilized by the loop connecting $\beta 7$ and $\beta 8$ (hereafter denoted L3) and two additional disulfide bridges (Cys42–Cys75, Cys55–Cys63). Closer inspection of the *Cmu1*–*ZmKWL1* interaction interface showed that *ZmKWL1* contacts *Cmu1* at four distinct sites. The N-terminal $\beta 1/\beta 2$ region interacts with helices $\alpha 1$ and $\alpha 5$ of *Cmu1* (Fig. 2c, left side). The L1 loop (connecting the β -strands $\beta 3$ and $\beta 4$) and the L3 loop (connecting the β -strands $\beta 7$ and $\beta 8$) bind to a large interface formed by helices $\alpha 1$ and $\alpha 7$ of *Cmu1* (Fig. 2c, left). Whereas L1 primarily interacts with helix $\alpha 7$, L3 protrudes in a plug-like manner into the active site of *Cmu1*. Last, the loop region connecting $\beta 4$ and $\beta 5$ (denoted L2) of *ZmKWL1* interacts with the tip of the ELR of *Cmu1* (Fig. 2c, right). The interaction interface of *ZmKWL1* at *Cmu1* could also be analysed in solution by hydrogen–deuterium exchange mass spectrometry (Extended Data Fig. 4a). Together, our structural analysis of the *Cmu1*–*ZmKWL1* complex shows that *ZmKWL1* forms a dense network of interactions with *Cmu1*, thereby probably blocking substrate access to the active site of *Cmu1*.

Increasing concentrations of *ZmKWL1* led to a decrease in chorismate mutase activity of *Cmu1* but not of *Aro7p* (Fig. 2d). Kinetic analysis of *Cmu1* in the presence of stoichiometric amounts of *ZmKWL1* showed a substantial decrease in the maximal velocity (V_{\max}) of

Cmu1 (40.8 ± 2.4 and $21.2 \pm 1.7 \mu\text{mol min}^{-1} \text{mg}^{-1}$ for *Cmu1* and *Cmu1*–*ZmKWL1*, respectively) (Fig. 2e). However, *ZmKWL1* did not markedly affect substrate binding to *Cmu1*, as indicated by an unaltered Michaelis–Menten constant (K_m) (0.8 ± 0.1 and $0.83 \pm 0.15 \text{ mM}$ for *Cmu1* and *Cmu1*–*ZmKWL1*, respectively) (Fig. 2e). These data substantiate our structural data, showing that *ZmKWL1* decreases the chorismate mutase activity of *Cmu1* in a non-competitive and allosteric manner. Next we created a *Cmu1* variant lacking a substantial portion of its ELR (*Cmu1*– ΔELR ; Extended Data Fig. 4b). *ZmKWL1* was unable to interact with *Cmu1*– ΔELR and it did not affect the chorismate mutase activity of *Cmu1*– ΔELR (Extended Data Fig. 5). This illustrates that *ZmKWL1* impairs substrate access to the active site of *Cmu1* through intimate interactions involving structural features that are specific to secreted fungal *Cmu1* proteins (Extended Data Fig. 4b). In vivo, the recognition of *Cmu1* by *ZmKWL1* is likely to happen in the apoplast, because *ZmKWL1* harbours an N-terminal signal peptide and can be secreted when transiently expressed in *N. benthamiana* (Extended Data Fig. 5c). In the apoplast, *ZmKWL1* might not only decrease the chorismate mutase activity of *Cmu1*, but also limit its transport into the plant cytosol. Higher levels of chorismate mutase (*ZmCM2* + *Cmu1*) have been suggested to increase the cytosolic levels of chorismate, leading to a change in chorismate homeostasis between the cytosol and the chloroplast³ (Fig. 3a). However, future research is necessary to clarify whether this is the case.

Kiwellins are present in most plant species, with the notable exception of the Brassicaceae (for example, *Arabidopsis thaliana*) (Fig. 3b, Supplementary Data). Several members of the monocots, asterids and rosids encode for more than 20 kiwellins (Fig. 3b). The maize genome encodes 19 kiwellin proteins in addition to *ZmKWL1* (Extended Data Fig. 6, Supplementary Data). These different kiwellins share the conserved β -barrel core domain stabilized by disulfide bridges (Figs. 2b, 3c, Extended Data Fig. 6). Moreover, they harbour a putative signal sequence, which suggests that they are secreted into the apoplastic space. However, all regions in *ZmKWL1* that are required for its interaction with Cmu1 are highly variable among the different kiwellin proteins of maize (Fig. 3c). The investigation of three different paralogues of *ZmKWL1* shows that they are unable to interact with Cmu1 and cannot inhibit its chorismate mutase activity (Extended Data Fig. 7a–d). Therefore, we speculate that the other maize kiwellins might specifically target other, as yet unknown fungal effectors (Fig. 3a).

It was noted that kiwellin proteins share considerable structural similarity within their β -barrel domain to the barwin-like and the cerato-platanin proteins in plants and fungi, respectively (Extended Data Fig. 7e). Although little functional knowledge is available at present, barwin-like proteins have been shown to increase the resistance of plants towards certain pathogens^{14,15}. Our structural analysis shows that members of the barwin-like and the cerato-platanin protein families lack all regions that are necessary for the interaction of *ZmKWL1* with Cmu1, most importantly the β 1/ β 2 domain (Extended Data Fig. 7f, g). Despite those differences, these proteins might perform similar functions to those now ascribed to the kiwellin, *ZmKWL1*.

Thus far, kiwellin proteins have been poorly understood and recognized as important only for the development of human allergy to the kiwi fruit^{16,17}. This study now suggests that kiwellins can act as plant defence proteins, counteracting alien effector activity with high specificity. This idea is supported by transcriptome data derived from potato plants infected with the oomycete *Phytophthora infestans*^{18,19}, in which a potato kiwellin homologue is strongly upregulated. Similar upregulation of a kiwellin-encoding gene has also been observed upon the infection of husk tomato with adult whiteflies²⁰. Therefore, kiwellins might be widespread and versatile scaffold proteins that counteract secreted pathogen effectors.

Online content

Any methods, additional references, Nature Research reporting summaries, source data, statements of data availability and associated accession codes are available at <https://doi.org/10.1038/s41586-018-0857-9>.

Received: 1 February 2018; Accepted: 4 December 2018;
Published online: 16 January 2019

1. Lanver, D. et al. *Ustilago maydis* effectors and their impact on virulence. *Nat. Rev. Microbiol.* **15**, 409–421 (2017).
2. Matei, A. & Doehlemann, G. Cell biology of corn smut disease — *Ustilago maydis* as a model for biotrophic interactions. *Curr. Opin. Microbiol.* **34**, 60–66 (2016).
3. Djamei, A. et al. Metabolic priming by a secreted fungal effector. *Nature* **478**, 395–398 (2011).
4. Kumar, D. Salicylic acid signaling in disease resistance. *Plant Sci.* **228**, 127–134 (2014).
5. Bekal, S., Niblack, T. L. & Lambert, K. N. A chorismate mutase from the soybean cyst nematode *Heterodera glycines* shows polymorphisms that correlate with virulence. *Mol. Plant Microbe Interact.* **16**, 439–446 (2003).
6. Doyle, E. A. & Lambert, K. N. *Meloidogyne javanica* chorismate mutase 1 alters plant cell development. *Mol. Plant Microbe Interact.* **16**, 123–131 (2003).

7. Liu, T. et al. Unconventionally secreted effectors of two filamentous pathogens target plant salicylate biosynthesis. *Nat. Commun.* **5**, 4686 (2014).
8. Xue, Y., Lipscomb, W. N., Graf, R., Schnappauf, G. & Braus, G. The crystal structure of allosteric chorismate mutase at 2.2-Å resolution. *Proc. Natl Acad. Sci. USA* **91**, 10814–10818 (1994).
9. Sträter, N., Schnappauf, G., Braus, G. & Lipscomb, W. N. Mechanisms of catalysis and allosteric regulation of yeast chorismate mutase from crystal structures. *Structure* **5**, 1437–1452 (1997).
10. Lanver, D. et al. The biotrophic development of *Ustilago maydis* studied by RNA-seq analysis. *Plant Cell* **30**, 300–323 (2018).
11. Mei, Y., Zhang, C., Kernodle, B. M., Hill, J. H. & Whitham, S. A. A *Foxtail mosaic virus* vector for virus-induced gene silencing in maize. *Plant Physiol.* **171**, 760–772 (2016).
12. Bölker, M., Genin, S., Lehmler, C. & Kahmann, R. Genetic regulation of mating and dimorphism in *Ustilago Maydis*. *Can. J. Bot.* **73**, 320–325 (1995).
13. Di Stasio, M., Brefort, T., Mendoza-Mendoza, A., Münch, K. & Kahmann, R. The dual specificity phosphatase Rok1 negatively regulates mating and pathogenicity in *Ustilago maydis*. *Mol. Microbiol.* **73**, 73–88 (2009).
14. Franco, F. P. et al. The sugarcane defense protein SUGARWIN2 causes cell death in *Colletotrichum falcatum* but not in non-pathogenic fungi. *PLoS ONE* **9**, e91159 (2014).
15. Wang, N., Xiao, B. & Xiong, L. Identification of a cluster of PR4-like genes involved in stress responses in rice. *J. Plant Physiol.* **168**, 2212–2224 (2011).
16. Offermann, L. R. et al. Elusive structural, functional, and immunological features of Act d 5, the green kiwifruit kiwellin. *J. Agric. Food Chem.* **63**, 6567–6576 (2015).
17. Hamiaux, C. et al. Crystal structure of kiwellin, a major cell-wall protein from kiwifruit. *J. Struct. Biol.* **187**, 276–281 (2014).
18. Draffehn, A. M. et al. Comparative transcript profiling by SuperSAGE identifies novel candidate genes for controlling potato quantitative resistance to late blight not compromised by late maturity. *Front. Plant Sci.* **4**, 423 (2013).
19. Mosquera, T. et al. Targeted and untargeted approaches unravel novel candidate genes and diagnostic SNPs for quantitative resistance of the potato (*Solanum tuberosum* L.) to *Phytophthora infestans* causing the late blight disease. *PLoS ONE* **11**, e0156254 (2016).
20. Quintana-Camargo, M. et al. Identification of genes differentially expressed in husk tomato (*Physalis philadelphica*) in response to whitefly (*Trialeurodes vaporariorum*) infestation. *Acta Physiol. Plant.* **37**, 29 (2015).

Acknowledgements We thank S. A. Whitham for the FoMV silencing system, V. Vincon for help in scoring the VIGS experiment and C. Pellegrin for interpreting RNA sequencing data. G.B. acknowledges support by the Deutsche Forschungsgemeinschaft (DFG) through the DFG-core facility for interactions, dynamics and macromolecular assembly structure and the Collaborative Research Council SFB987. F.A. and X.H. were supported by the Peter and Traudl Engelhorn foundation and the China Scholarship Council (CSC), respectively. R.K. acknowledges generous support by the Max Planck Society. We thank the European Synchrotron Radiation Facility (ESRF) for support.

Reviewer information Nature thanks N. Talbot and the other anonymous reviewer(s) for their contribution to the peer review of this work.

Author contributions X.H. conducted in vivo experiments, western blotting and enzyme kinetic analysis. T.G. identified proteins by mass spectrometry. F.A. and J.S. determined all crystal structures. W.S. analysed the *ZmKWL1*/Cmu1 complex by hydrogen–deuterium exchange mass spectrometry. F.A. and L.B. performed pull-down analysis. P.I.G. performed isothermal titration calorimetry analysis. A.D. provided the relevant material. S.A.R. performed phylogenetic analysis. R.K., S.R. and G.B. planned experiments, analysed data and supervised the project. R.K. and G.B. wrote the manuscript. All authors read and commented on the manuscript.

Competing interests The authors declare no competing interests.

Additional information

Extended data is available for this paper at <https://doi.org/10.1038/s41586-018-0857-9>.

Supplementary information is available for this paper at <https://doi.org/10.1038/s41586-018-0857-9>.

Reprints and permissions information is available at <http://www.nature.com/reprints>.

Correspondence and requests for materials should be addressed to R.K. or G.B. **Publisher's note:** Springer Nature remains neutral with regard to jurisdictional claims in published maps and institutional affiliations.

METHODS

No statistical methods were used to predetermine sample size. The experiments were not randomized and the investigators were not blinded to allocation during experiments and outcome assessment.

Strains, growth conditions and plant infection assays. The *Escherichia coli* strain Top10 (Life Technologies) was used for cloning purposes. *E. coli* strains BL21(DE3) (Promega) and SHuffle T7 (New England Biolabs) were used for expression of recombinant Cmu1, ZmCM1, ZmCM2, ZmCM3 and the maize kiwellin proteins, respectively. *U. maydis* strains used in this study are listed in Extended Data Table 2. *Agrobacterium tumefaciens* GV3101²¹ was used for transient expression of ZmKWL1 in *N. benthamiana*. *Z. mays* cv. Early Golden Bantam (EGB, Urban Farmer) was grown in a temperature-controlled greenhouse (light and dark cycles of 14 h at 28 °C and 10 h at 20 °C, respectively) and used for infection by *U. maydis*. *N. benthamiana* was grown in a phytochamber (light and dark cycles of 16 h at 25 °C and 8 h at 22 °C, respectively). *U. maydis* strains were grown in YEPSL (0.4% (w/v) yeast extract, 0.4% (w/v) peptone and 2% (w/v) sucrose) and cell suspensions in double-distilled water adjusted to an OD₆₀₀ of 1.0 were injected into the stem of 7-day-old maize seedlings with a syringe as described²².

Molecular cloning of plasmids. For plasmid constructions, standard molecular cloning strategies and techniques were applied²³. All plasmids and primers used in this study are listed in Extended Data Tables 2, 3. For overexpression of Cmu1 in *E. coli*, plasmid pET28a-Cmu1 was generated. To do so, the *cmu1* gene without the signal peptide (Cmu1^{22–290}) was codon-optimized for *E. coli* expression and inserted into the NdeI/XhoI site of pET28a (Novagen). To generate plasmid pET28a-Cmu1-ΔELR, DNA fragments for Cmu1^{22–116} and Cmu1^{141–290} were amplified from pET28a-Cmu1 and then ligated with pET28a-Cmu1 digested with NdeI/XhoI via Gibson Assembly according to the manufacturer's protocol (New England Biolabs). The ZmKWL1 gene was amplified from genomic DNA of EGB and inserted into pJET1.2/blunt (Thermo Scientific), producing pJET1-ZmKWL1. For ZmKWL1 overexpression in *E. coli*, its coding sequence lacking the signal peptide (ZmKWL1^{33–198}) was amplified from pJET1-ZmKWL1 and inserted into the NdeI/XhoI sites of pET28a, yielding pET28a-ZmKWL1. For constitutive overexpression of Cmu1 in *U. maydis*, plasmid p123²⁴ containing the constitutive *otef* promoter was digested with XmaI/AflII and ligated with a *cmu1*-HA₃ DNA fragment that was amplified by PCR from p123-P_{cmu1}-Cmu1-HA₃³, yielding p123-P_{otef}-Cmu1-HA₃. To generate p123-P_{otef}-Cmu1-ΔELR-HA₃, *cmu1*-ΔELR-HA₃ was amplified by PCR from p123-P_{cmu1}-Cmu1-ΔELR-HA₃ (X. Han and R. Kahmann, unpublished results) and inserted into XmaI/AflII sites of p123. For transient overexpression of ZmKWL1 in *N. benthamiana*, pEZRK-ZmKWL1-His₆ was constructed by inserting ZmKWL1 gene amplified by PCR from pJET1-ZmKWL1 into KpnI/XbaI sites of pEZRK-LCY (courtesy of D. Ehrhardt, Stanford University), which carries the CaMV 35S promoter. For localization of ZmKWL1 in *N. benthamiana*, DNA fragments encoding ZmKWL1-sfGFP and ZmKWL1^{ΔSP}-sfGFP were amplified from p35S-ZmKWL1-sfGFP (X. Han and R. Kahmann, unpublished results). The resulting products were inserted into KpnI/XbaI sites of pEZRK-LCY, respectively. All amplified segments of plasmids were sequenced.

Generation of *U. maydis* strains. *U. maydis* AB33 strain²⁵ was used to constitutively overexpress Cmu1 in axenic culture. Plasmids p123-P_{otef}-Cmu1-HA₃ and p123-P_{otef}-Cmu1-ΔELR-HA₃ were integrated into the *ip* locus of AB33 as described previously²⁶. Isolated *U. maydis* transformants were confirmed by Southern blot analysis to obtain single integration events in the *ip* locus.

Protein production and purification. Cmu1 and ZmKWL1 used for crystal structure determination and biochemical assays were always expressed without the signal peptide (compare to section 'Molecular cloning of plasmids'). Cmu1, ZmCM1, ZmCM2 and ZmCM3 (without the predicted signal peptide) were produced by incubating plasmid-containing *E. coli* BL21 (DE3) in lysogeny broth (LB)-medium supplemented with 12.5 g l⁻¹ D-(+)-lactose monohydrate and 50 μg ml⁻¹ kanamycin for 16 h at 30 °C under rigorous shaking. To produce kiwellin proteins from *Z. mays* without the native signal peptides, *E. coli* SHuffle T7 cells carrying the plasmid were grown in LB-medium supplemented with 50 μg ml⁻¹ kanamycin at 30 °C and rigorously shaken until an optical density of 0.6 was obtained. After addition of 0.5 mM IPTG, the cells were further grown for 20 h at 16 °C. All *E. coli* cells were collected by centrifugation (3,500g, 20 min, 4 °C), resuspended in lysis buffer (20 mM of HEPES-Na pH 8.0, 250 mM NaCl, 20 mM MgCl₂, 20 mM KCl supplemented 40 mM imidazole) and lysed through a M-110L microfluidizer (Microfluidics). The cell debris was removed by centrifugation (47,850g, 20 min, 4 °C) and the clear supernatant loaded on a 5-ml HisTrap column (GE Healthcare) equilibrated with 10 column volumes of lysis buffer. After washing with 10 column volumes of lysis buffer, the proteins were eluted with 3 column volumes of elution buffer (lysis buffer containing 500 mM imidazole). Proteins were concentrated (Amicon Ultracel-10K, Millipore) and subjected to size-exclusion chromatography (SEC) on a HiLoad 26/600 Superdex 200 pg column (GE Healthcare) equilibrated with SEC buffer (20 mM of HEPES-Na, pH 7.5, 200 mM NaCl 20 mM MgCl₂ and 20 mM KCl). Protein-containing fractions were pooled and concentrated in

Amicon Ultracel-10K cells (Millipore). Protein concentration was determined by a spectrophotometer (NanoDrop Lite, Thermo Scientific). We reconstituted the Cmu1-ZmKWL1 complex by mixing both proteins in a 1:2 ratio and subjecting the mixture to SEC (HiLoad 26/600 Superdex 200 pg column (GE Healthcare)). Fractions containing the Cmu1-ZmKWL1 complex were pooled and concentrated.

Crystallization and structure determination. Crystallization was performed by the sitting-drop method at 20 °C in 0.5 μl drops consisting of equal parts of protein and precipitation solutions. Cmu1 crystallized at a concentration of 20 mg ml⁻¹ within one week in 0.2 M MES pH 5.0, 20% (w/v) PEG 6000. The Cmu1-ZmKWL1 complex crystallized at a concentration of 15 mg ml⁻¹ within four days in 0.1 M sodium citrate pH 5.5, 15% (w/v) PEG 6000. ZmCM1 crystallized at a concentration of 15 mg ml⁻¹ in 0.2 M ammonium tartrate and 20% (w/v) PEG 3350 after one week. ZmCM2 crystals were observed within one week in 0.2 M sodium acetate and 24% (w/v) PEG 4000. Before data collection, crystals were flash-frozen in liquid nitrogen using a cryo-solution that consisted of mother liquor supplemented with 20% (v/v) glycerol. Data were collected under cryogenic conditions at the European Synchrotron Radiation Facility. The data for the crystals of Cmu1 and Cmu1-ZmKWL1 were collected at 0.987 Å on ID23-1, while the data for ZmCM1 and ZmCM2 were collected at 0.8762 Å on ID23-2. Data were processed with XDS²⁷ and CCP4-implemented AIMLESS²⁸. The Cmu1 structure was determined by single-wavelength anomalous dispersion using selenomethionine-labelled protein crystals. The substructure was determined with the CCP4-implemented program CRANK²⁹. The structure of Cmu1-ZmKWL1 was determined by molecular replacement with PHASER³⁰ using the structures of Cmu1 (this study) and the kiwi fruit protein, KWL1 (PDB: 4PMK¹⁷) as search models. The structures of ZmCM1 and ZmCM2 were solved by molecular replacement using the chorismate mutase from *A. thaliana* (PDB: 4PPU) as a search model. All structures were manually built in Coot³¹, and refined with PHENIX³². Ramachandran statistics for the final model of Cmu1 show 97.44% of residues in the most favourable regions, 2.46% in allowed regions and 0.10% outliers. The statistical values for the final models of Cmu1-ZmKWL1, ZmCM1 and ZmCM2 were 27.81%/2.19%/0%, 96.21%/3.58%/0.21% and 97.74%/2.26%/0%, respectively. Figures were prepared with PyMOL (<https://www.pymol.org>) and Chimera³³.

Chorismate mutase activity assay. Kinetic analysis of Cmu1 and inhibition of Cmu1 by ZmKWL1 was carried out with a previously described 'online assay'³⁴. The assay monitored the disappearance of the substrate chorismate at a wavelength of 274 nm (OD₂₇₄; the extinction coefficient of chorismate is $\epsilon_{274\text{ nm}} = 2,630\text{ M}^{-1}\text{ cm}^{-1}$). The OD₂₇₄ was measured using TECAN Infinite 200 PRO plate reader (Tecan Trading AG). Standard assays were performed at 30 °C in 250 μl of reaction buffer composed of 40 mM Tris-HCl (pH 7.0) and 100 mM NaCl. In a standard reaction, chorismate mutase activity was measured with 100 ng of Cmu1 protein (that is, 13 nM concentration) and 0.5 mM chorismate (Sigma). Initial velocity was calculated from the linear decrease of OD₂₇₄. The kinetic data were fitted to the Michaelis-Menten equation using SigmaPlot (Systat Software). The decrease of OD₂₇₄ of chorismate in the absence of enzyme during the time course was subtracted as the blank value.

Transient expression of proteins in *N. benthamiana*. *A. tumefaciens* GV3101 strains carrying respective pEZRK plasmids were grown in LB-medium containing appropriate antibiotics (50 μg ml⁻¹ kanamycin, 50 μg ml⁻¹ rifampicin and 50 μg ml⁻¹ gentamicin) to an OD₆₀₀ of 1.0. After washing three times with double-distilled water, the cell pellet was suspended in MES buffer (10 mM MES, 10 mM MgCl₂, 100 μM acetosyringone) to an OD₆₀₀ of 0.25. The GV3101 cell suspension was incubated at 18 °C overnight and infiltrated into the lower side of four-week old *N. benthamiana* leaves using a 1 ml syringe without needle. Three days after infiltration, *N. benthamiana* leaves were excised for protein analysis or localization of ZmKWL1-sfGFP using confocal microscopy¹⁰.

Co-immunoprecipitation assay. *U. maydis* AB33 strains overexpressing Cmu1-HA₃ or Cmu1-ΔELR-HA₃ were grown in complete medium supplemented with 2% (w/v) glucose³⁵. When OD₆₀₀ reached 0.8–1.0, the culture was collected by centrifugation. The supernatant was concentrated 100-fold using Amicon Ultracel-10K (Millipore) to 500 μl. Agroinfiltrated *N. benthamiana* leaves were collected three days after infiltration and ground in liquid nitrogen. HNN extraction buffer (50 mM HEPES-Na pH 7.5, 150 mM NaCl, 50 mM NaF, 5 mM EDTA, 0.1% (v/v) NP-40, 1% (w/v) polyvinylpyrrolidone (PVP), 0.5% (w/v) sodium deoxycholate, 1x cComplete protease inhibitor cocktail (Roche) was added to the ground powder and incubated for 15 min on ice. Following centrifugation (16,000g, 20 min, 4 °C), 500 μl of the clarified plant lysate and the concentrated supernatant of *U. maydis* culture were mixed with 50 μl Ni-NTA agarose (Qiagen). The mixture was incubated at 4 °C for approximately 16 h under constant rotation. The beads were washed three times with the extraction buffer followed by the addition of 100 μl SDS loading buffer (1% (v/v) β-mercaptoethanol, 0.004% (w/v) bromophenol blue, 6% (v/v) glycerol, 2% (w/v) sodium dodecyl sulfate, 50 mM Tris-HCl pH 6.8) and boiling for 10 min. After brief centrifugation, the supernatant was analysed by SDS-PAGE and western blot.

FoMV-mediated VIGS in maize. The 300-bp silencing fragment targeting *ZmKWL1* was designed with the SGN VIGS tool (<http://vigs.solgenomics.net/>) and corresponds to nucleotides 181 to 480 of the *ZmKw1* gene. The VIGS construct pFoMV-*ZmKWL1*¹⁸¹⁻⁴⁸⁰ was generated by inserting the silencing fragment into XbaI/XhoI sites of the Foxtail mosaic virus vector pFoMV-V in the antisense orientation¹¹. To propagate viral sap for rub-inoculation, the first leaf of a six-day-old maize seedling was transformed via biolistic transformation (PDS-1000/He system, Bio-Rad). Gold particles (1.6 µm) were coated with pFoMV-*ZmKWL1*¹⁸¹⁻⁴⁸⁰ and pFoMV-V DNA and bombardment was performed at 1,100 psi in a 90-kPa vacuum chamber. Ten days after bombardment, viral sap was prepared by grinding leaves showing infection symptoms in phosphate-buffered saline (137 mM NaCl, 2.7 mM KCl, 10 mM Na₂HPO₄, 1.8 mM KH₂PO₄, pH 7.4). Six-day-old maize seedlings were rub-inoculated using Silicon carbide powder (600-mesh, Alfa Aesar) with the viral sap containing either pFoMV-V or pFoMV-*ZmKWL1*¹⁸¹⁻⁴⁸⁰. To test the effects of silencing on virulence, the rub-inoculated maize plants were infected 6 days after the rub-inoculation by *U. maydis* strain CL13 and disease symptoms were scored 12 days after *U. maydis* inoculation. To check the silencing efficiency, 6 cm leaf segments with viral symptom were collected from pFoMV-V or pFoMV-*ZmKWL1*¹⁸¹⁻⁴⁸⁰ infected maize plants 6 days after virus infection. Total RNA was extracted with TRIzol (Invitrogen), treated with TURBO DNA-free Kit (Ambion) and subsequently applied to cDNA synthesis using Superscript III First Strand Synthesis SuperMix (Invitrogen). qPCR reactions were carried out as previously described¹⁰ using primer pairs XW234/XW235 for *ZmKWL1* and GAPDH-F/R for the maize GAPDH gene (Extended Data Table 3).

Identification of *ZmKWL1* by liquid chromatography–mass spectrometry. Anti-HA magnetic beads (10 µl) were added to the lysate of *Z. mays* leaves three days post infection with the *U. maydis* strain SG200Dcmu1-Cmu1-HA3 and incubated for 2 h at 4 °C on a rotator. The beads were washed four times with 700 µl 100 mM ammonium bicarbonate, and 100 µl elution buffer 1 (1.6 M urea, 100 mM ammonium bicarbonate, 10 µg ml⁻¹ trypsin (Promega)). After 30 min incubation at 27 °C, the supernatant containing the digested proteins was collected. Beads were washed twice with elution buffer 2 (1.6 M urea, 100 mM ammonium bicarbonate, 1 mM TCEP) and added to the first elution fraction. Digest was allowed to proceed overnight at room temperature. After digest the beads were incubated with 5 mM iodoacetamide at 30 min at 25 °C in the dark. The sample was acidified using trifluoroacetic acid and peptides were purified using C18 Microspin columns (Harvard Apparatus) according to the manufacturer's instructions. Dried peptides were reconstituted in 0.1% trifluoroacetic acid and then analysed using liquid-chromatography–mass spectrometry carried out on a Q-Exactive Plus instrument connected to an Ultimate 3000 RSLC nano and a nanospray flex ion source (all Thermo Scientific). Peptide separation was performed on a reverse phase HPLC column (75 µm × 42 cm) packed in-house with C18 resin (2.4 µm; Dr. Maisch). The following separating gradient was used: 98% solvent A (0.15% formic acid) and 2% solvent B (99.85% (v/v) acetonitrile, 0.15% (w/v) formic acid) to 32% solvent B over 60 min and to 50% B for an additional 20 min at a flow rate of 300 nl min⁻¹. The data acquisition mode was set to obtain one high resolution MS scan at a resolution of 70,000 full width at half maximum (at *m/z* 200) followed by MS/MS scans of the 10 most intense ions. To increase the efficiency of MS/MS attempts, the charged state screening modus was enabled to exclude unassigned and singly charged ions. The dynamic exclusion duration was set to 30 s. The ion accumulation time was set to 50 ms (MS) and 50 ms at 17,500 resolution (MS/MS). The automatic gain control was set to 3 × 10⁶ for MS survey scan and 1 × 10⁵ for MS/MS scans. For the database search, the protein database for *U. maydis* and *Z. mays* was downloaded from Uniprot (<https://www.uniprot.org>, downloaded October 2015) and the search was performed using the combined protein databases. The search of the mass spectrometry raw data was performed on Mascot (Version 2.5, Matrix Science). The search criteria were set as follows: full tryptic specificity was required (cleavage after lysine or arginine residues); two missed cleavages were allowed; carbamidomethylation (C) was set as a fixed modification; oxidation (M) was set as a variable modification. The mass tolerance was set to 10 p.p.m. for precursor ions and 0.02 Da for fragment ions. The search results were then loaded into Scaffold (Proteome Software) and 1% protein false discovery rate was adjusted.

Hydrogen–deuterium exchange mass spectrometry (HDX-MS). Samples for hydrogen–deuterium exchange–mass spectrometry (HDX-MS) measurements were automatically prepared by a two-arm robotic autosampler (LEAP Technologies). A volume of 7.5 µl (40 µM) Cmu1 or the Cmu1–*ZmKWL1* complex were mixed with 67.5 µl of D₂O-containing SEC buffer to start the HDX reaction. After 10/30/95/1,000/10,000 s incubation at 25 °C, 55 µl of the HDX reaction was added to 55 µl quench buffer (400 mM KH₂PO₄/H₃PO₄, 2 M guanidine-HCl, pH 2.2) kept at 1 °C and 95 µl of the resulting mixture immediately injected into an ACQUITY UPLC M-class system with HDX technology (Waters)³⁶. Peptide generation was carried out online with immobilized pepsin at 12 °C and a 100 µl min⁻¹ flow rate of water + 0.1% (v/v) formic acid and the peptic peptides trapped on a C18 column (Waters) kept at 0.5 °C for 3 min. Afterwards, the trap column

was placed in line with an ACQUITY UPLC BEH C18 1.7 µm 1.0 × 100 mm column (Waters) and the peptides eluted at 0.5 °C using a gradient of water + 0.1% (v/v) formic acid (eluent A) and acetonitrile + 0.1% (v/v) formic acid (eluent B) at a flow rate of 30 µl min⁻¹: 0–7 min/95–65% A, 7–8 min/65–15% A, 8–10 min/15% A, 10–11 min/5% A, 11–16 min/95% A. Mass spectra of deuterated Cmu1 were acquired in HDMS (high definition MS) positive ion mode using a G2-Si HDMS mass spectrometer equipped with an electrospray ionization source (Waters). Non-deuterated samples of Cmu1 were prepared by a similar procedure using non-deuterated SEC-buffer and mass spectra acquired in HDMS^E (enhanced high definition MS) mode^{37,38}. Lock mass correction was performed using [Glu1]-Fibrinopeptide B standard (Waters). The pepsin column was washed with 80 µl of 4% (v/v) acetonitrile and 0.5 M guanidine-HCl three times during each run. All measurements were performed in triplicate. Blank runs were performed between each sample to avoid peptide carry-over. Peptide identification and assignment of deuterium incorporation was carried out as described previously^{39–41} aided by PLGS and DynamX 3.0 softwares (Waters).

Phylogenetic analysis. The *ZmKWL1* amino acid sequence was used as query to blast fully-sequenced genomes of plants, algae and fungi. Blast hits were filtered according to ref.⁴², in order to retain homologous sequences only. Multiple sequence alignment was generated using MAFFT linsi⁴³ and manually curated using Jalview⁴⁴, removing sequences covering less than 50 per cent of the conserved positions as well as alignment columns of low quality. Tree inference was conducted using Bayesian inference with MrBayes⁴⁵. The appropriate prior model was selected on the basis of AIC/BIC using Prottest⁴⁶ and turned out to be WAG+G. Bayesian inference was run with two hot and two cold chains for 20 million generations (standard deviation of split frequencies 0.114; 500 trees were discarded as burn-in). Phylogenetic trees were visualized using FigTree v1.4.3 (<http://tree.bio.ed.ac.uk/software/figtree/>; Supplementary Data). All sequences confirmed as kiwellins via the phylogenetic inference were counted for the bar chart representation in Fig. 3b. The fungal sequences form a clade that is distinct from the plant sequences, not suggesting horizontal gene transfer.

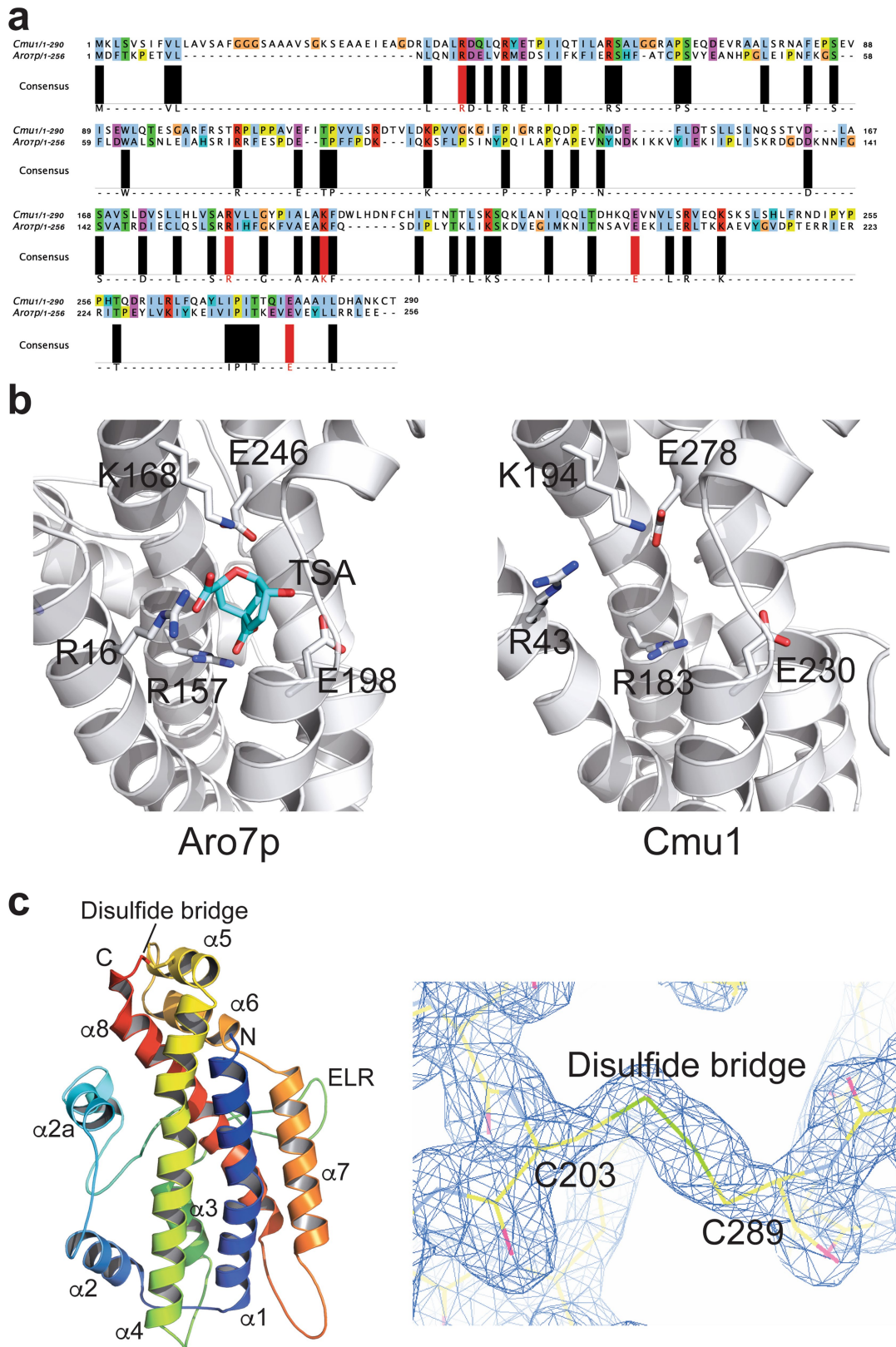
Reporting summary. Further information on research design is available in the Nature Research Reporting Summary linked to this article.

Data availability

Coordinates and structure factors were deposited at the Protein Data Bank (PDB) under the accession codes 6FPF, 6FPG, 6HJW and 6H3P for Cmu1, the Cmu1–*ZmKWL1* complex, *ZmCM1* and *ZmCM2*, respectively. Extended Data Figs. 3, 5, 7 have associated source data. The data that support the findings of this study are available from the corresponding authors upon reasonable request.

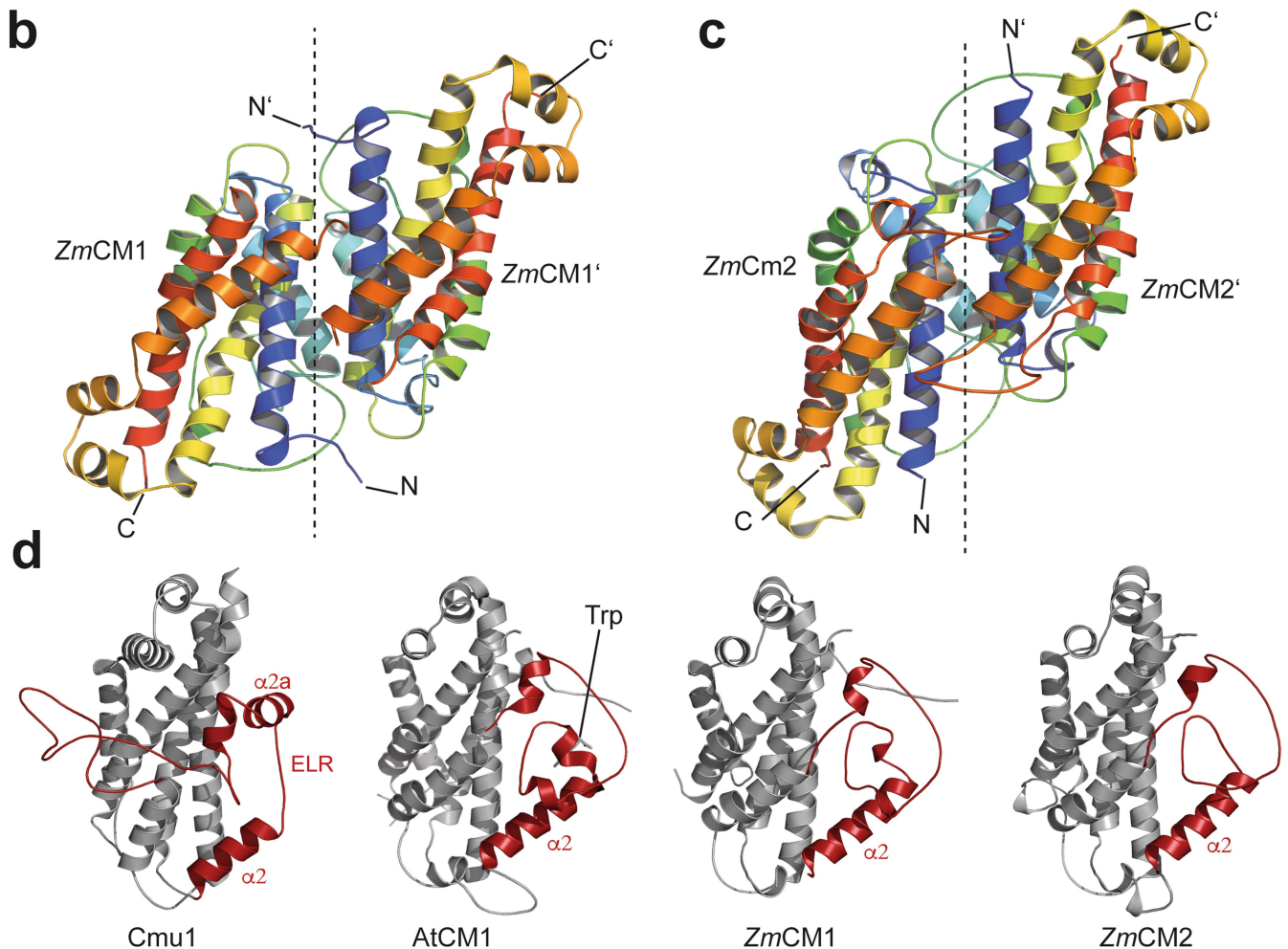
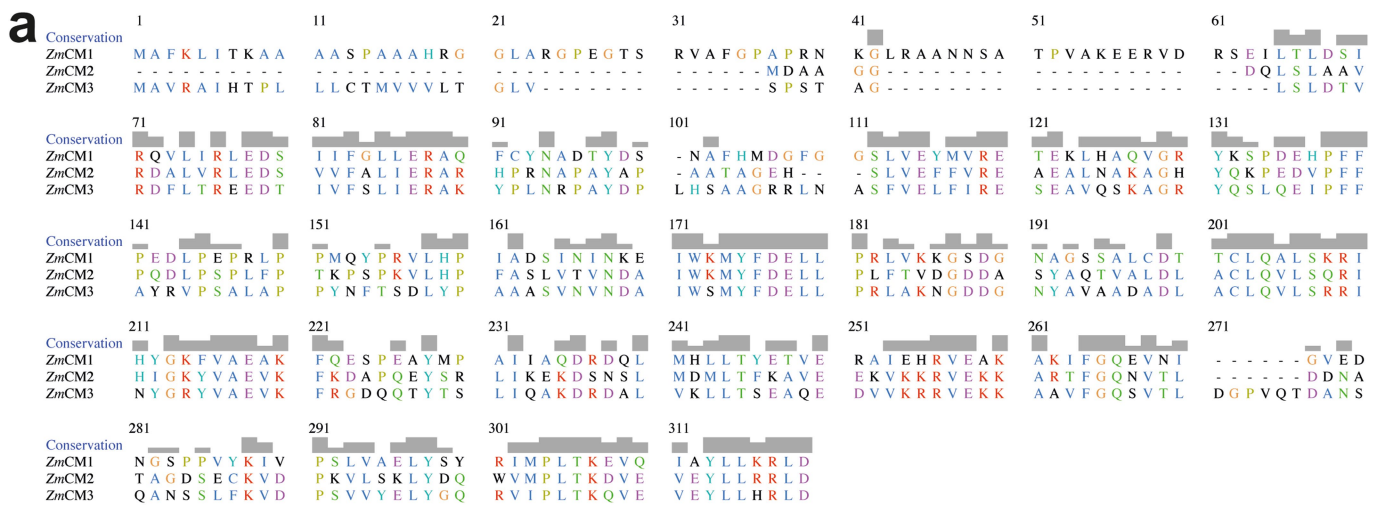
- Koncz, C. & Schell, J. The promoter of T₁-DNA gene 5 controls the tissue-specific expression of chimaeric genes carried by a novel type of *Agrobacterium* binary vector. *Mol. Genet. Genomics* **204**, 383–396 (1986).
- Kämper, J. et al. Insights from the genome of the biotrophic fungal plant pathogen *Ustilago maydis*. *Nature* **444**, 97–101 (2006).
- Sambrook, J., Fritsch, E. F. & Maniatis, T. *Molecular cloning: a laboratory manual* 2nd edn (Cold Spring Harbor Laboratory, New York, 1989).
- Müller, P., Weinzierl, G., Brachmann, A., Feldbrügge, M. & Kahmann, R. Mating and pathogenic development of the Smut fungus *Ustilago maydis* are regulated by one mitogen-activated protein kinase cascade. *Eukaryot. Cell* **2**, 1187–1199 (2003).
- Brachmann, A., Weinzierl, G., Kämper, J. & Kahmann, R. Identification of genes in the bW/bE regulatory cascade in *Ustilago maydis*. *Mol. Microbiol.* **42**, 1047–1063 (2001).
- Loubradou, G., Brachmann, A., Feldbrügge, M. & Kahmann, R. A homologue of the transcriptional repressor Ssn6p antagonizes cAMP signalling in *Ustilago maydis*. *Mol. Microbiol.* **40**, 719–730 (2001).
- Kabsch, W. Xds. *Acta Crystallogr. D* **66**, 125–132 (2010).
- Evans, P. R. & Murshudov, G. N. How good are my data and what is the resolution? *Acta Crystallogr. D* **69**, 1204–1214 (2013).
- Pannu, N. S. et al. Recent advances in the CRANK software suite for experimental phasing. *Acta Crystallogr. D* **67**, 331–337 (2011).
- McCoy, A. J. et al. Phaser crystallographic software. *J. Appl. Crystallogr.* **40**, 658–674 (2007).
- Emsley, P. & Cowtan, K. Coot: model-building tools for molecular graphics. *Acta Crystallogr. D* **60**, 2126–2132 (2004).
- Adams, P. D. et al. PHENIX: a comprehensive Python-based system for macromolecular structure solution. *Acta Crystallogr. D* **66**, 213–221 (2010).
- Pettersen, E. F. et al. UCSF Chimera—a visualization system for exploratory research and analysis. *J. Comput. Chem.* **25**, 1605–1612 (2004).
- Sasso, S., Ramakrishnan, C., Gampfer, M., Hilvert, D. & Kast, P. Characterization of the secreted chorismate mutase from the pathogen *Mycobacterium tuberculosis*. *FEBS J.* **272**, 375–389 (2005).
- Holliday, R. Molecular aspects of genetic exchange and gene conversion. *Genetics* **78**, 273–287 (1974).
- Wales, T. E., Fadgen, K. E., Gerhardt, G. C. & Engen, J. R. High-speed and high-resolution UPLC separation at zero degrees Celsius. *Anal. Chem.* **80**, 6815–6820 (2008).

37. Geromanos, S. J. et al. The detection, correlation, and comparison of peptide precursor and product ions from data independent LC-MS with data dependant LC-MS/MS. *Proteomics* **9**, 1683–1695 (2009).
38. Li, G. Z. et al. Database searching and accounting of multiplexed precursor and product ion spectra from the data independent analysis of simple and complex peptide mixtures. *Proteomics* **9**, 1696–1719 (2009).
39. Schäper, S. et al. AraC-like transcriptional activator CuxR binds c-di-GMP by a PiiZ-like mechanism to regulate extracellular polysaccharide production. *Proc. Natl Acad. Sci. USA* **114**, E4822–E4831 (2017).
40. Schuhmacher, J. S. et al. MinD-like ATPase FlhG effects location and number of bacterial flagella during C-ring assembly. *Proc. Natl Acad. Sci. USA* **112**, 3092–3097 (2015).
41. Steinchen, W. et al. Catalytic mechanism and allosteric regulation of an oligomeric (p)ppGpp synthetase by an alarmone. *Proc. Natl Acad. Sci. USA* **112**, 13348–13353 (2015).
42. Rost, B. Twilight zone of protein sequence alignments. *Protein Eng.* **12**, 85–94 (1999).
43. Katoh, K. & Standley, D. M. MAFFT multiple sequence alignment software version 7: improvements in performance and usability. *Mol. Biol. Evol.* **30**, 772–780 (2013).
44. Waterhouse, A. M., Procter, J. B., Martin, D. M., Clamp, M. & Barton, G. J. Jalview Version 2—a multiple sequence alignment editor and analysis workbench. *Bioinformatics* **25**, 1189–1191 (2009).
45. Ronquist, F. et al. MrBayes 3.2: efficient Bayesian phylogenetic inference and model choice across a large model space. *Syst. Biol.* **61**, 539–542 (2012).
46. Darriba, D., Taboada, G. L., Doallo, R. & Posada, D. ProtTest 3: fast selection of best-fit models of protein evolution. *Bioinformatics* **27**, 1164–1165 (2011).
47. Edgar, R. C. MUSCLE: a multiple sequence alignment method with reduced time and space complexity. *BMC Bioinformatics* **5**, 113 (2004).
48. Edgar, R. C. MUSCLE: multiple sequence alignment with high accuracy and high throughput. *Nucleic Acids Res.* **32**, 1792–1797 (2004).
49. Li, W. et al., The EMBL-EBI bioinformatics web and programmatic tools framework. *Nucleic Acids Res.* **43**, W580–W584 (2015).
50. Holm, L. & Rosenstrom, P. Dali server: conservation mapping in 3D. *Nucleic Acids Res.* **38**, W545–W549 (2010).
51. Huet, J. et al. High-resolution structure of a papaya plant-defense barwin-like protein solved by in-house sulfur-SAD phasing. *Acta Crystallogr. D* **69**, 2017–2026 (2013).
52. Karniel, A. et al. Co-translational folding intermediate dictates membrane targeting of the signal recognition particle receptor. *J. Mol. Biol.* **430**, 1607–1620 (2018).



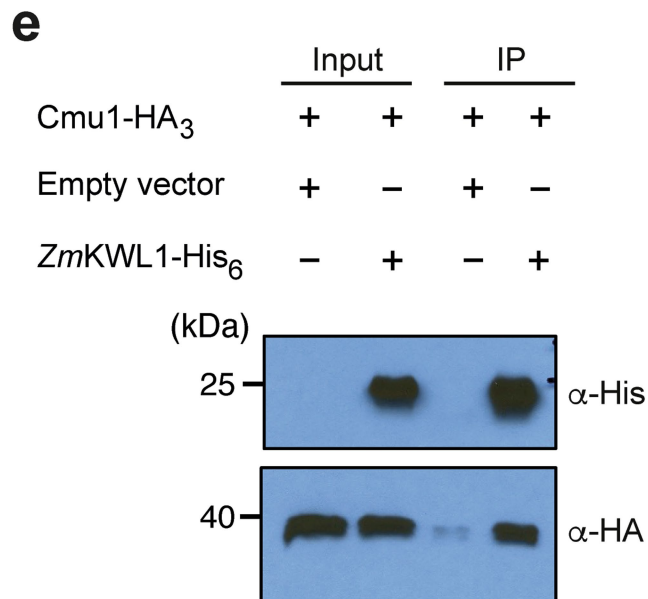
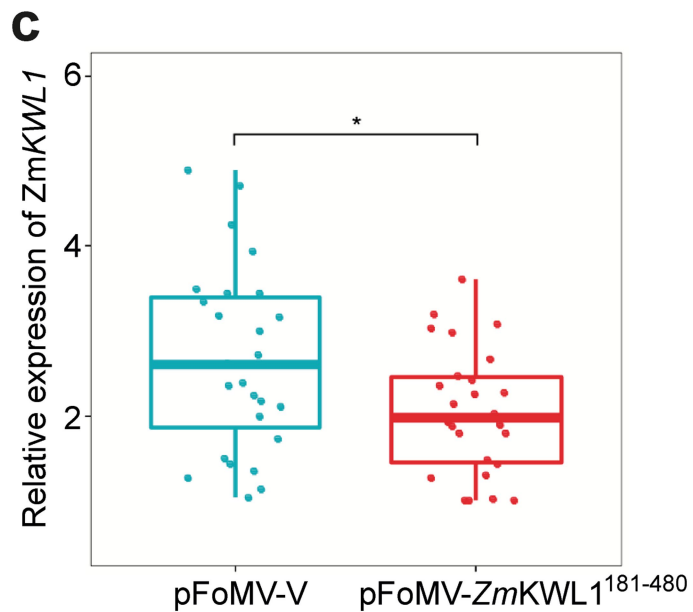
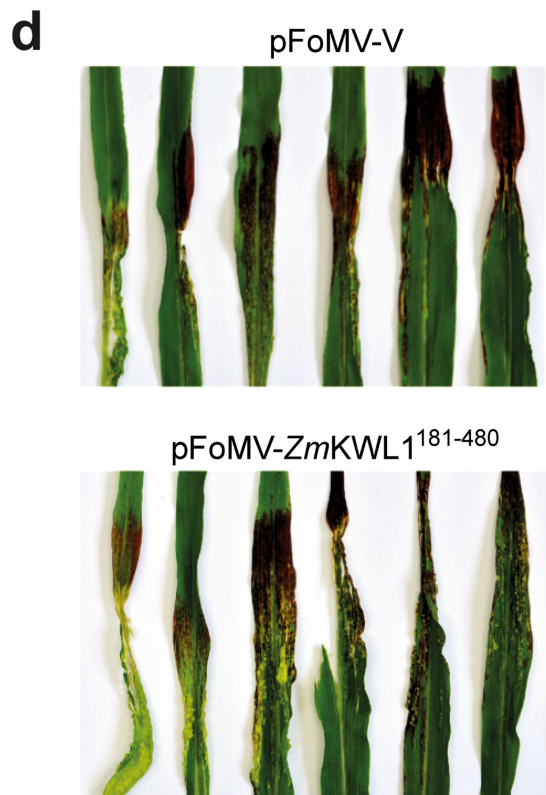
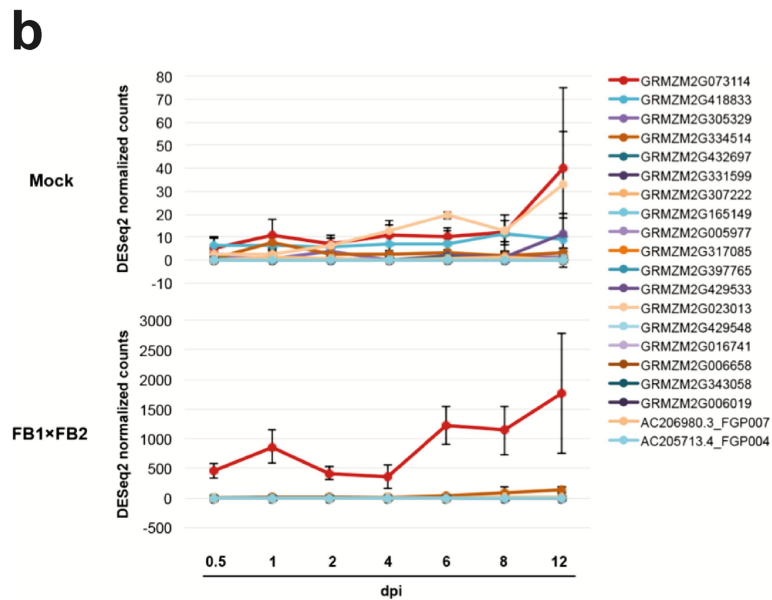
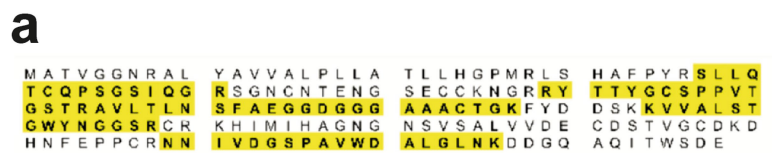
Extended Data Fig. 1 | Comparison of Cmu1 and Aro7p. a, Sequence alignment of Aro7p and Cmu1. Conserved active site residues are coloured in red. **b**, Side-by-side view of the active sites of Aro7p and Cmu1 shows that all residues that are critical for substrate binding and catalysis are conserved. To prepare the figure, the structures of Aro7p (left; PDB: 3CSM⁹ and Cmu1 (right; this study) were superimposed. Aro7p is in complex with an *endo*-oxabicyclic transition state analogue inhibitor

(TSA). **c**, Left, cysteine residues 203 and 289 of Cmu1 form a disulfide bridge linking helix $\alpha 5$ and the C terminus. Right, the $2F_o - F_c$ electron density map at a 1.6σ cut-off around the disulfide bridge. It is of note that both cysteines are highly conserved among Cmu1 homologues from plant-pathogenic fungi and are not found in housekeeping chorismate mutases, such as Aro7p (see a).



Extended Data Fig. 2 | Comparison of chorismate mutases of the maize plant. **a**, Sequence alignment of *Zea mays* chorismate mutases. The alignment was generated with MUSCLE^{47–49}, with residues colour-coded according to their chemical properties, and the table was generated in Chimera³³. **b**, **c**, Crystal structures of *ZmCM1* from the chloroplast (**b**)

and *ZmCM2* from the cytoplasm (**c**) of *Z. mays* (this study). A dashed line divides the homodimer of each structure. Both structures show the conserved chorismate mutase fold, including an allosteric loop. **d**, Comparison between Cmu1, CM1 from *A. thaliana* (*At*) (PDB: 4PPU), *ZmCM1* and *ZmCM2*. The ELR and allosteric loop are highlighted in red.



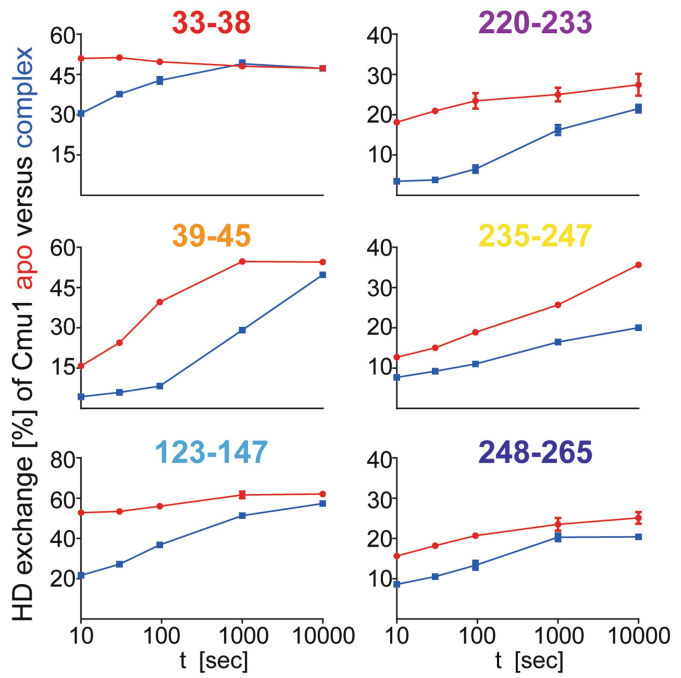
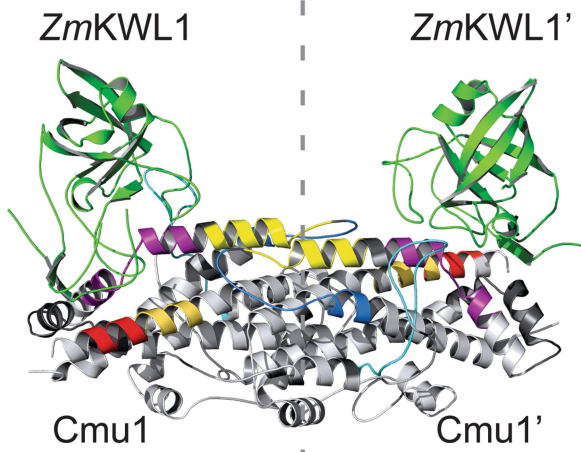
Extended Data Fig. 3 | See next page for caption.

Extended Data Fig. 3 | *Z. mays* KWL1 interacts with *U. maydis* Cmu1 in vivo and in vitro and is involved in infection of maize by *U. maydis*.

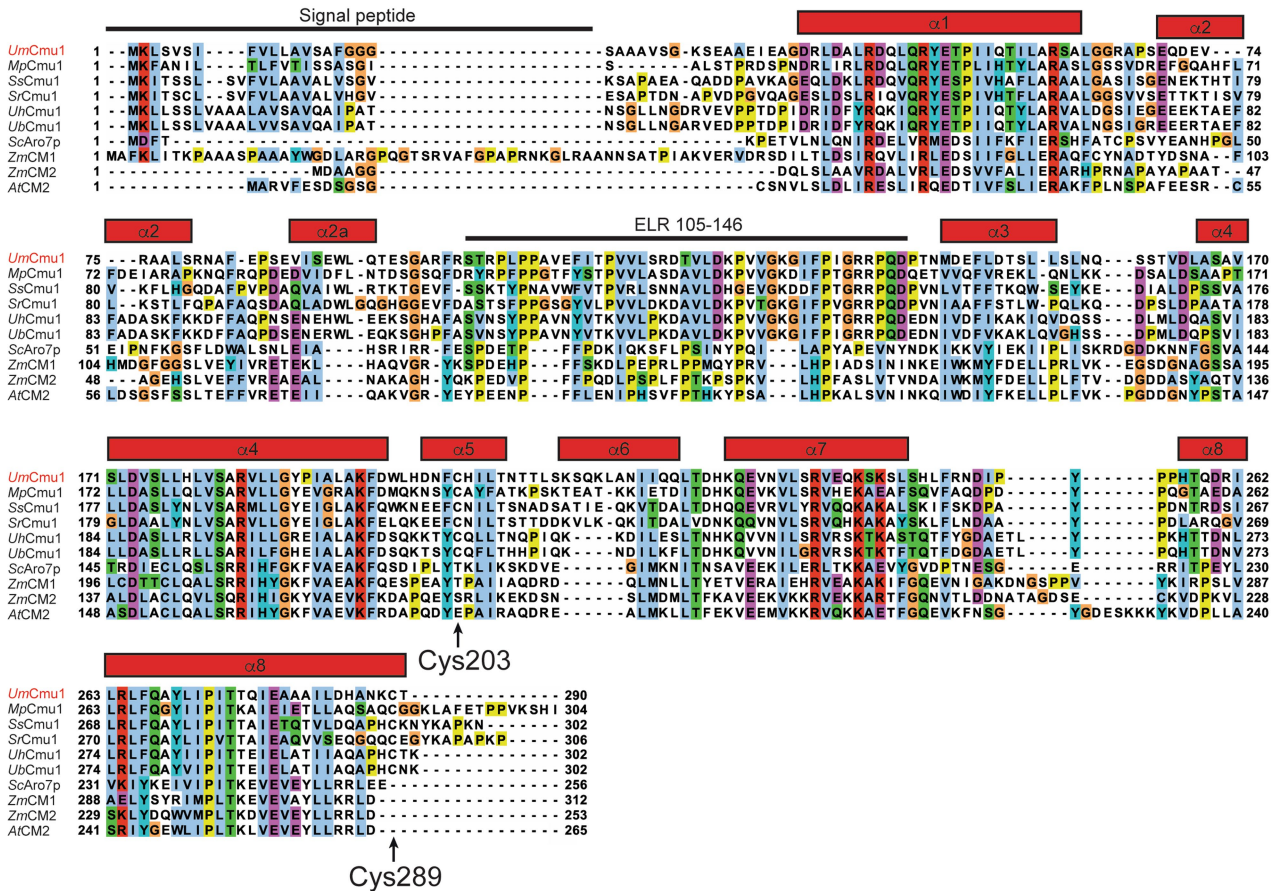
a, Mass spectrometry unambiguously identified the hypothetical maize protein with the annotation GRMZM2G073114 (*ZmKWL1*). The protein was identified by several unique spectra of peptides (indicated in yellow) covering 44 per cent of the total sequence. **b**, Relative expression levels of 20 maize kiwellin genes during biotrophic development of *U. maydis* were revealed by RNA sequencing analysis of RNA samples collected from mock (top) and FB1 × FB2 (bottom) infected maize plants (dataset available via ref. ¹⁰ and GEO accession number GSE103876). The vertical axis indicates normalized counts from DESeq2 analysis. The horizontal axis indicates the infection stages: 0.5, 1, 2, 4, 6, 8 and 12 days post infection (dpi). Data represent mean ± s.d. of $n = 3$ biological replicates. Colour codes for different genes are indicated in the legend. **c**, Six-day-old maize seedlings were rub-inoculated with virus-sap containing pFoMV-V and pFoMV-*ZmKWL1*¹⁸¹⁻⁴⁸⁰, respectively. Twenty-seven leaves from three biological replicates were analysed six days after viral inoculation and expression of *ZmKWL1* was analysed separately in each leaf by qPCR using the maize gene *GAPDH*, which encodes glyceraldehyde-3-phosphate-dehydrogenase, as internal reference. Boxplot representation

indicates that expression levels of *ZmKWL1* in pFoMV-*ZmKWL1*¹⁸¹⁻⁴⁸⁰ infected maize leaves were reduced compared to expression levels in pFoMV-V infected plants, indicative of silencing. A total of 27 leaves from $n = 3$ biological replicates were assessed. The centre line of the box plot denotes the median, lower and upper box hinges represent first and third quartiles, respectively, and whiskers indicate the maximum and minimum values. *P* value was determined by unpaired two-sided Student's *t*-test. * $P = 0.0202$. **d**, Maize plants silenced for *ZmKWL1* via infection with pFoMV-*ZmKWL1*¹⁸¹⁻⁴⁸⁰ (left) and non-silenced plants infected with pFoMV-V (right) were infected with CL13 strain. Representative leaves with heaviest *U. maydis* infection symptoms were imaged 12 days after CL13 infection. Representative experiments are shown. The experiment was repeated independently twice with similar results. **e**, Supernatant of AB33-p123-P_{otef}-Cmu1-HA₃ containing Cmu1-HA₃ was incubated with Ni-NTA agarose and plant lysates of *N. benthamiana* leaves infiltrated with GV3101 transformed with empty vector pEZRK-LCY or pEZRK-*ZmKWL1*-His₆. *ZmKWL1* and Cmu1 were detected by western blot using His antibody (top) and HA antibody (bottom), respectively. Representative images are displayed. The experiment was repeated independently once with similar results.

a



b

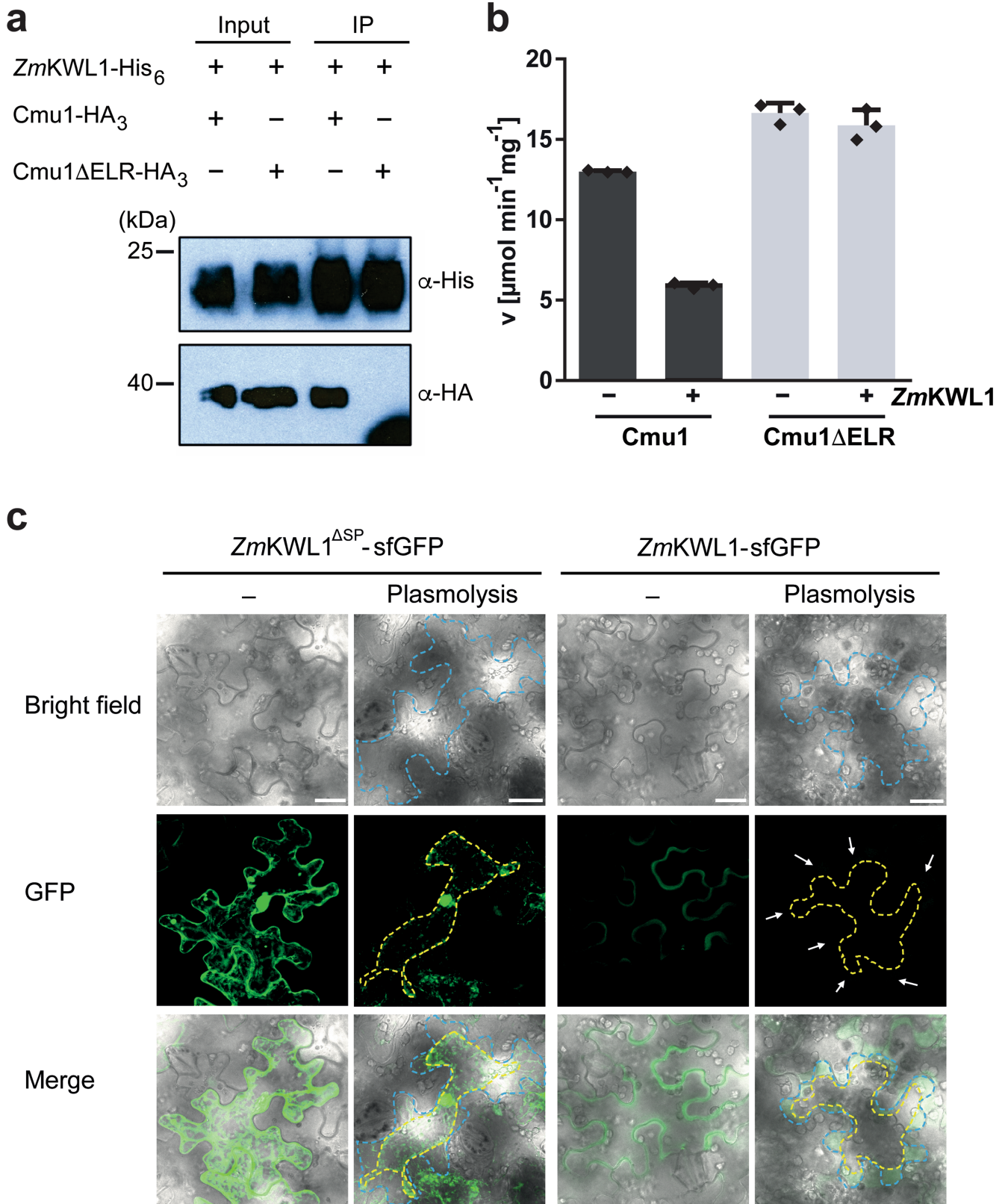


Extended Data Fig. 4 | See next page for caption.

Extended Data Fig. 4 | The ZmKWL1 interaction site at Cmu1 is specific for secreted chorismate mutases from plant-pathogenic fungi.

a, Left, representative regions of Cmu1 lining the interaction interface are indicated in the crystal structure of the Cmu1–ZmKWL1 complex. Right, deuterium uptake plots of representative regions of Cmu1 alone (red) and the Cmu1–ZmKWL1 complex (blue). Data represent mean \pm s.d. of $n = 3$ technical replicates. **b**, Amino acid sequences of chorismate mutases from the plant-pathogenic fungi *Ustilago maydis* (UmCmu1), *Melanopsichium pennsylvanicum* (MpCmu1), *Sporisorium scitamineum* (SsCmu1), *Sporisorium reilianum* (SrCmu1), *Ustilago hordei* (UhCmu1), *Ustilago bromivora* (UbCmu1) and chorismate mutases from the non-pathogenic

species *Saccharomyces cerevisiae* (ScAro7p), *Zea mays* (ZmCM1 and ZmCM2) and *A. thaliana* (AtCM2) were aligned with MUSCLE^{47–49}. Conserved amino acid residues are colour-coded according to their polarity and charge. The secondary structure of UmCmu1 (this study) is displayed above the alignment. The disulfide-bond-forming cysteine residues Cys203 and Cys289 (numbering according to UmCmu1) found in plant-pathogenic fungi are indicated. Chorismate mutases critically differ in the region between helices $\alpha 2$ and $\alpha 3$. In plant-pathogenic fungi, the additional helix $\alpha 2a$ and an extended loop region (ELR, numbering according to UmCmu1) are present.



Extended Data Fig. 5 | See next page for caption.

Extended Data Fig. 5 | Prerequisites of Cmu1 for the Cmu1–KWL1 interaction and localization of ZmKWL1. **a**, *ZmKWL1* is unable to interact with the Cmu1- Δ ELR variant. Supernatant of AB33-p123- P_{otef} -Cmu1-HA₃ or AB33-p123- P_{otef} -Cmu1- Δ ELR-HA₃ containing Cmu1-HA₃ or Cmu1- Δ ELR-HA₃, was incubated with Ni-NTA agarose and plant lysate of *N. benthamiana* leaves infiltrated with GV3101 transformed with pEZRK-*ZmKWL1*-His₆. After co-immunoprecipitation, *ZmKWL1* and Cmu1 were detected by western blot using antibodies against His₆ (*ZmKWL1*, top) or HA₃ (Cmu1, bottom), respectively. Representative images are displayed. The experiment was repeated independently once with similar results. **b**, *ZmKWL1* inhibits the chorismate mutase activity of Cmu1 but not of Cmu1 that lacks the ELR (Cmu1- Δ ELR). Chorismate mutase activity was determined with the chorismate mutase activity assay. Data represent mean \pm s.d. of $n = 3$ technical replicates.

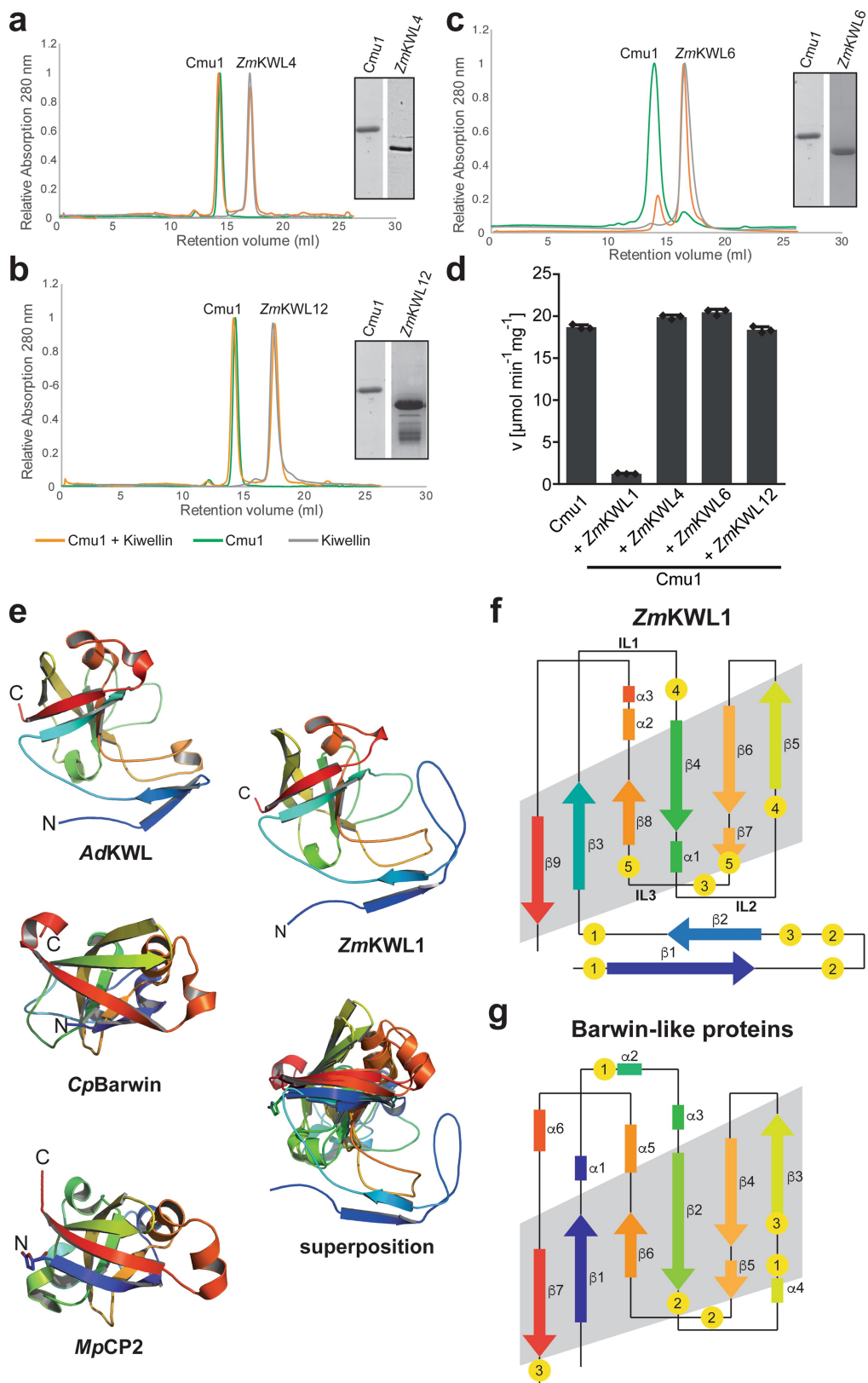
c, To investigate the localization of *ZmKWL1*, we transiently expressed *ZmKWL1*-sfGFP fusion proteins with (*ZmKWL1*-sfGFP) and without signal peptide (*ZmKWL1* $^{\Delta$ SP-sfGFP) using *A. tumefaciens* for delivery. *ZmKWL1* $^{\Delta$ SP-sfGFP mainly accumulated in the cytosol and the nucleus. After plasmolysis with 1 M NaCl, the fluorescence signal pattern remained unchanged. By contrast, *ZmKWL1*-sfGFP with its native signal peptide showed peripheral localization and the signal accumulated in the enlarged apoplastic space after plasmolysis. This observation demonstrates the secretion of *ZmKWL1* into the apoplast. The dashed blue line marks the plant cell wall and the dashed yellow line marks the plant plasma membrane. Arrows mark the enlarged apoplast in which the secreted *ZmKWL1*-sfGFP protein accumulates. Scale bars, 25 μ m. Representative images are displayed. The experiment was repeated independently once with similar results.



* Residues at *ZmKw1* involved in *Cmu1* interaction
 not resolved
 β-strand
 α-helix

Extended Data Fig. 6 | Amino acid sequence alignment of different kiwellin paralogs from *Z. mays*. Amino acid sequences from *Z. mays* kiwellins were aligned with MUSCLE^{47–49}. The secondary structure of *ZmKw1* (GRMZM2G073114) is displayed according to the crystal

structure. Conserved residues are colour-coded according to their polarity and charge. Kiwellin homologues are highly conserved in their β-barrel domains. Five kiwellins show similarity to the β1/β2 region of *ZmKw1*. Four kiwellins carry C-terminal extensions.



Extended Data Fig. 7 | See next page for caption.

Extended Data Fig. 7 | Interaction of different maize kiwellins with Cmu1 and similarities among kiwellins, barwin-like proteins and cerato-platanin. **a**, *ZmKWL4* (GRMZM2G432697) migrates with an apparent molecular mass of 15 kDa, which corresponds to a monomer (calculated molecular mass: 17 kDa), whereas Cmu1 migrates with the apparent molecular mass of a dimer. When *ZmKWL4* and Cmu1 were mixed in a 2:1 ratio, no complex formation was observed. **b**, *ZmKWL12* (GRMZM2G429533) migrates with an apparent molecular mass of 15 kDa, which corresponds to a monomer (calculated molecular mass: 17 kDa), whereas Cmu1 migrates with the apparent molecular mass of a dimer. When *ZmKWL12* and Cmu1 were mixed in a 2:1 ratio, no complex formation was observed. **c**, *ZmKw6* (GRMZM2G331599) migrates with an apparent molecular mass of 13 kDa which corresponds to a monomer (calculated molecular mass: 14 kDa), while Cmu1 migrates with the apparent molecular mass of a dimer. When *ZmKw6* and Cmu1 were mixed in a 2:1 ratio, again no complex formation was observed. In **a–c**, the insets show a Coomassie-stained SDS-PAGE of the peak fraction. Each experiment was repeated twice with similar results. **d**, Activity of Cmu1 is inhibited by *ZmKWL1* but not by *ZmKWL4*, *ZmKWL6* or *ZmKWL12*. Data represent mean \pm s.d. of $n = 3$ technical replicates. **e**, The crystal structures of two kiwellin proteins from *Actinidia chinensis* (PDB: 4PMK¹⁷) and *Actinidia deliciosa* (*AdKWL*, PDB: 4X9U¹⁶) superimpose very well with the structure of *ZmKWL1* with root mean

square deviations (r.m.s.d.) of 0.42 Å and 0.40 Å over 119 C α -atoms and 110 C α -atoms, respectively (alignment not shown). Search with the DALI-server⁵⁰ revealed members of the barwin and CP-proteins as structurally similar to *ZmKWL1*. The structure of a barwin-like protein from *Carica papaya* (*CpBarwin*, PDB: 4JP6⁵¹) superposes well with *ZmKWL1* (r.m.s.d.: 0.92 Å over all C α -atoms). The β -barrel domain of *ZmKWL1* and the barwin-like protein formed by six β -strands can be perfectly superposed. The β 1/ β 2-domain of *ZmKWL1*, however, is absent in barwin-like proteins. Moreover, several loops critical for the recognition of Cmu1 by *ZmKWL1* are considerably reduced in length in the barwin-like proteins or completely absent. The structure of a cerato-platanin protein from *Moniliophthora perniciosa* (*MpCP2*, PDB: 3SUK) also shares the β -barrel with the kiwellins and barwin-like proteins and aligns well with *ZmKWL1* (r.m.s.d.: 1.11 Å over all C α -atoms). Our structural comparison of the barwin-like proteins with the cerato-platanin shows that both proteins are highly similar. This suggests to us that barwin-like proteins and cerato-platanins are, in structural terms, members of the same protein family. All structures are shown as cartoons and are rainbow-coloured from their N- to their C termini. **f**, **g**, Topology of *ZmKWL1* (**f**) and a Barwin-like protein (**g**). The structure of both proteins is coloured in rainbow from blue (N-terminal) to red (C-terminal). A yellow circle indicates individual cysteines, and disulfide bond numbers (1–5, as above) are indicated.

Extended Data Table 1 | Data collection and refinement statistics

	Cmu1-ZmKWL1	Cmu1 Se-Met SAD	ZmCM1	ZmCM2
Data collection				
Space group	<i>P</i> 1	<i>P</i> 2 ₂ 1 ₂ 1	<i>C</i> 22 ₂ 1	<i>P</i> 3 ₂ 21
Cell dimensions				
<i>a</i> , <i>b</i> , <i>c</i> (Å)	59.51, 85.66, 95.79	82.77, 83.48, 186.73	61.8, 89.83, 216.84	162.59, 162.59, 55.38
α , β , γ (°)	96.16, 92.39, 90.37	90.00, 90.00, 90.00	90.00, 90.00, 90.00	90.00, 90.00, 120.00
Wavelength (Å)		Peak 0.987		
Resolution (Å)	49.00 – 1.80 (1.83 – 1.80)	49.74 – 1.90 (1.93 – 1.90)	44.92 – 2.50 (2.58 – 2.50)	45.77 - 2.70 (2.79 – 2.70)
<i>R</i> _{merge}	0.041 (0.472)	0.083 (0.773)	0.096 (1.018)	0.342 (1.628)
<i>I</i> / σ <i>I</i>	11.2 (1.6)	11.1 (1.8)	12.46 (1.56)	7.26 (1.34)
Completeness (%)	96.6 (95.1)	99.5 (90.8)	99.69 (99.48)	99.92 (99.91)
Redundancy	2.9 (2.9)	6.7 (6.3)	6.6 (6.3)	11.4 (10.9)
Refinement				
Resolution (Å)	48.50 - 1.80	49.74 – 2.20	44.82 – 2.50	45.77 - 2.70
No. reflections	168242 (16605)	66423 (6532)	24182 (2289)	23338 (2320)
<i>R</i> _{work} / <i>R</i> _{free}	18.6 / 21.5	16.5 / 20.3	22.2 / 27.4	18.4 / 23.1
No. atoms	14061	8957	3992	4043
Protein	12838	8121	3973	3890
Ligand/ion	52	1	0	0
Water	1171	835	19	153
<i>B</i> -factors				
Protein	40.37	35.55	72.54	43.85
Ligand/ion	47.16	57.86	-	-
Water	44.07	39.53	56.03	39.50
R.m.s. deviations				
Bond lengths (Å)	0.023	0.030	0.004	0.011
Bond angles (°)	1.58	2.42	0.98	1.33

Values in parentheses are for the highest-resolution shell. Data were collected from one crystal for each dataset.

Extended Data Table 2 | Strains and plasmids used in the study

Strain	Genotype	Reference
AB33	a2: <i>P_{nar}: bW2 bE1</i>	(25)
CL13	a1: <i>bW2 bE1</i>	(12)
SG200Dcmu1-Cmu1-HA ₃	a1: <i>mfa2 bW2 bE1 Dum05731 ip^R[P_{um05731}-um05731]ip^S</i>	(F. Hartwig and R. Kahmann, unpublished)
AB33-p123-P _{otef} -Cmu1-HA ₃	a2: <i>P_{nar}: bW2 bE1 ip^R[P_{otef}-um05731]ip^S</i>	This study
AB33-p123-P _{otef} -Cmu1-DEL- HA ₃	a2: <i>P_{nar}: bW2 bE1 ip^R[P_{otef}-um05731^{Δ117-140}]ip^S</i>	This study
Strain	Usage	Reference
pET28a	Protein overexpression	Novagen
pET24d	Protein overexpression	Novagen
pEMGB1	Protein overexpression	(52)
pET28a-Cmu1	For recombinant overexpression of Cmu1 in <i>E. coli</i>	This study
pET28a-Cmu1-ΔELR	For recombinant overexpression of Cmu1- DEL in <i>E. coli</i>	This study
pJET1.2/blunt		Thermo Scientific
pJET1-ZmKw1	Template for the amplification of the maize <i>ZmKw1</i> gene	This study
pET28a-ZmKw1	For recombinant overexpression of <i>ZmKw1</i> in <i>E. coli</i>	This study
p123		(24)
p123-P _{cmu1} -Cmu1-HA ₃		(3)
p123-P _{cmu1} -Cmu1-DEL- HA ₃		(X. Han and R. Kahmann, unpublished)
p123-P _{otef} -Cmu1-HA ₃	For constitutive overexpression of Cmu1 in <i>U. maydis</i>	This study
p123-P _{otef} -Cmu1-DEL- HA ₃	For constitutive overexpression of Cmu1- DEL in <i>U. maydis</i>	This study
pEZRK-LCY		Courtesy of Dr. Ehrhardt, Stanford, USA
pEZRK-ZmKw1-His ₆	For overexpression of <i>ZmKw1</i> -His ₆ in <i>N. benthamiana</i>	This study
p35S-ZmKw1-sfGFP		(X. Han and R. Kahmann, unpublished)
pEZRK-ZmKw1-sfGFP	For localization of <i>ZmKw1</i> in <i>N. benthamiana</i>	This study
pEZRK-ZmKw1 ^{ΔSP} -sfGFP	For localization of <i>ZmKw1</i> in <i>N. benthamiana</i>	This study
pET24d-ZmKw14	For recombinant overexpression of <i>ZmKw14</i> in <i>E. coli</i>	This study
pEMGB1-ZmKw16	For recombinant overexpression of <i>ZmKw16</i> in <i>E. coli</i>	This study
pEMGB1-ZmKw12	For recombinant overexpression of <i>ZmKw12</i> in <i>E. coli</i>	This study
pET24d-ZmCm1	For recombinant overexpression of <i>ZmCm1</i> in <i>E. coli</i>	This study
pET24d-ZmCm2	For recombinant overexpression of <i>ZmCm2</i> in <i>E. coli</i>	This study
pET24d-ZmCm3	For recombinant overexpression of <i>ZmCm3</i> in <i>E. coli</i>	This study
pFoMV-V		Courtesy of Dr. Whitham, Iowa, USA
pFoMV-ZmKw1 ¹⁸¹⁻⁴⁸⁰	For silencing of <i>ZmKw1</i> in maize	(11) This study

See refs 3,11,12,24,25,52.

Extended Data Table 3 | Primers used in the study

Primer	Sequence (5' to 3')	Restriction site	Usage
XW034	GAGCCCGGGATGAAGTTGAGCGTGTC	<i>XmaI</i>	Cloning <i>cmu1</i> to p123 (F)
AD214	CATCGCAAGACCGGCAACAGGATTC	-	Cloning <i>cmu1</i> to p123 (R)
XW135	ATGGCTACCGTCGGGGCAATCGTGCTCT C	-	Cloning <i>ZmKWL1</i> to pJET1.2/blunt (F)
XW136	TCACTCGTCGGACCAGGTGATCTGTGCC	-	Cloning <i>ZmKWL1</i> to pJET1.2/blunt (R)
XW139	CGCGGTACCATGGCTACCGTCGGGGGCA ATC	<i>KpnI</i>	Cloning <i>ZmKWL1</i> to pEZRK-LCY (F)
XW140	CGCTCTAGATCAGTGGTGGTGGTGGTGGT GCTCGTCGGACCAGGTGATCTG	<i>XbaI</i>	Cloning <i>ZmKWL1</i> to pEZRK-LCY (R)
XW142	AAACATATGTTCCCATACCGTTCCTACTC	<i>NdeI</i>	Cloning <i>ZmKWL1</i> to pET28a (F)
XW143	TTTCTCGAGCTCGTCGGACCAGGTGATCT G	<i>XhoI</i>	Cloning <i>ZmKWL1</i> to pET28a (R)
XW150	CTTTAAGAAGGAGATATCATATGGCTGCTG TTTCTGGTAAATC	-	Cloning <i>cmu1</i> ²²⁻¹¹⁶ to pET28a (F)
XW151	CGGAGAGCCAGAGCCCGGGGTGATGAAT TCAAC	-	Cloning <i>cmu1</i> ²²⁻¹¹⁶ to pET28a (R)
XW152	TCACCCCGGGCTCTGGCTCTCCGCAGGAC CCGACCAAC	-	Cloning <i>cmu1</i> ¹⁴¹⁻²⁹⁰ to pET28a (F)
XW153	CAGTGGTGGTGGTGGTGGTGGTGGTGGTGGT TGCATTTGTTAGCGTGG	-	Cloning <i>cmu1</i> ¹⁴¹⁻²⁹⁰ to pET28a (R)
XW185	AAATCTAGATTACTTGTAGAGTTCGTCCAT GCC	<i>XbaI</i>	Cloning <i>ZmKWL1</i> -sfGFP to pEZRK-LCY (R)
XW186	AAAGGTACCATGTCTGAAGGGCGAGGAACT CTTC	<i>KpnI</i>	Cloning <i>ZmKWL1</i> -sfGFP to pEZRK-LCY (F)
XW215	GACGGTACCATGTTCCCATACCGTTCCT ACTC	<i>KpnI</i>	Cloning <i>ZmKWL1</i> ^{ΔSP} -sfGFP to pEZRK-LCY (F)
LB007	TTAACCATGGGCCACGTCCAAGTCTCC	<i>NcoI</i>	Cloning <i>ZmKWL4</i> to pET24d (F)
LB011	TCCTCGGATCCTTAGACATCAGACCAGGT	<i>BamHI</i>	Cloning <i>ZmKWL4</i> to pET24d (R)
LB015	TTAATCATGAGCCGGCACGGCAAGCCA	<i>BspHI</i>	Cloning <i>ZmKWL6</i> to pEMGB1 (F)
LB016	TCCTCGGATCCTTAATGGTGTGATGGTGTG GTGGCGTCGGACCACGTG	<i>BamHI</i>	Cloning <i>ZmKWL6</i> to pET24d (R)
LB018	TTAACCATGGGCCACCACCACCACCGG C	<i>NcoI</i>	Cloning <i>ZmKWL12</i> to pEMGB1 (F)
LB022	TTAAGGATCCTTAGGCGTCGGACCAGGT	<i>BamHI</i>	Cloning <i>ZmKWL12</i> to pET24d (R)
XW018	CTTCCATGGCCTTCAAGCTGATCACC	<i>NcoI</i>	Cloning <i>ZmCM1</i> into pET24d (F)
XW019	CGAACTCGAGATCCAGCCTCTTAAGC	<i>XhoI</i>	Cloning <i>ZmCM1</i> into pET24d (R)
XW020	GAACCATGGACGCGCGGGCGGCGACCA G	<i>NcoI</i>	Cloning <i>ZmCM2</i> into pET24d (F)
XW021	CGAACTCGAGGTCGAGGCGGCGCAGGAG ATAC	<i>XhoI</i>	Cloning <i>ZmCM2</i> into pET24d (R)
XW205	ATACCATGGGGCTCAGCCTGGACACG	<i>NcoI</i>	Cloning <i>ZmCM3</i> into pET24d (F)
XW206	GTGCTCGAGGTCGAGGCGATGGAGAAG	<i>XhoI</i>	Cloning <i>ZmCM3</i> into pET24d (R)
XW171	TAATCTAGAGTCCTTGTGCGAGCCCACGG TG	<i>XbaI</i>	Cloning silencing fragment of <i>ZmKWL1</i> to pFoMV-V (F)
XW172	TCGCTCGAGTCCGAGTGCTGCAAGAACGG GC	<i>XhoI</i>	Cloning silencing fragment of <i>ZmKWL1</i> to pFoMV-V (R)
XW234	AGTCGTCGCGCTGCCACTTC		qRT-PCR of <i>ZmKWL1</i> (F)
XW235	GGCTGGCAGGTCTGGAGTAG		qRT-PCR of <i>ZmKWL1</i> (R)
GAPDH-F	CTTCGGCATTGTTGAGGGTTTG		qRT-PCR of maize <i>GAPDH</i> gene (F)
GAPDH-R	TCCTTGCTGAGGGTCCGTC		qRT-PCR of maize <i>GAPDH</i> gene (R)

Reporting Summary

Nature Research wishes to improve the reproducibility of the work that we publish. This form provides structure for consistency and transparency in reporting. For further information on Nature Research policies, see [Authors & Referees](#) and the [Editorial Policy Checklist](#).

Statistical parameters

When statistical analyses are reported, confirm that the following items are present in the relevant location (e.g. figure legend, table legend, main text, or Methods section).

n/a Confirmed

- The exact sample size (n) for each experimental group/condition, given as a discrete number and unit of measurement
- An indication of whether measurements were taken from distinct samples or whether the same sample was measured repeatedly
- The statistical test(s) used AND whether they are one- or two-sided
Only common tests should be described solely by name; describe more complex techniques in the Methods section.
- A description of all covariates tested
- A description of any assumptions or corrections, such as tests of normality and adjustment for multiple comparisons
- A full description of the statistics including central tendency (e.g. means) or other basic estimates (e.g. regression coefficient) AND variation (e.g. standard deviation) or associated estimates of uncertainty (e.g. confidence intervals)
- For null hypothesis testing, the test statistic (e.g. F , t , r) with confidence intervals, effect sizes, degrees of freedom and P value noted
Give P values as exact values whenever suitable.
- For Bayesian analysis, information on the choice of priors and Markov chain Monte Carlo settings
- For hierarchical and complex designs, identification of the appropriate level for tests and full reporting of outcomes
- Estimates of effect sizes (e.g. Cohen's d , Pearson's r), indicating how they were calculated
- Clearly defined error bars
State explicitly what error bars represent (e.g. SD, SE, CI)

Our web collection on [statistics for biologists](#) may be useful.

Software and code

Policy information about [availability of computer code](#)

Data collection

CCP4i-suite including e.g. PHASER, COOT, aimless; Phenix-suite, XDS, Pymol, Chimera

Data analysis

Excel 2013 (Microsoft), DynamX 3.0 (Waters), PLGS 3.0.1 (Waters), GraphPad Prism 6.0.4 (GraphPad Software), Open-Source PYMOL 1.5.0.5 (Schrödinger), Chimera 1.12 (UCSF), SigmaPlot 13 (Systat Software), CCP4 7.0, Mascot 2.5 (Matrix Science), Scaffold 4 (Proteome Software), Muscle align (<https://www.ebi.ac.uk/Tools/msa/muscle/>), FigTree 1.4.3 (<http://tree.bio.ed.ac.uk/software/figtree/>), Jalview 2.10.0 (A. M. Waterhouse, J. B. Procter, D. M. Martin, M. Clamp, G. J. Barton, Jalview Version 2--a multiple sequence alignment editor and analysis workbench. *Bioinformatics* 25, 1189-1191 (2009).; <http://www.jalview.org/>), MAFFT linsi 7.037b (K. Katoh, D. M. Standley, MAFFT multiple sequence alignment software version 7: improvements in performance and usability. *Mol Biol Evol* 30, 772-780 (2013)), MrBayes 3.2.6 x64 (F. Ronquist et al., MrBayes 3.2: efficient Bayesian phylogenetic inference and model choice across a large model space. *Syst Biol* 61, 539-542 (2012)), Prottest 3.4.2 (D. Darriba, G. L. Taboada, R. Doallo, D. Posada, ProtTest 3: fast selection of best-fit models of protein evolution. *Bioinformatics* 27, 1164-1165 (2011))

For manuscripts utilizing custom algorithms or software that are central to the research but not yet described in published literature, software must be made available to editors/reviewers upon request. We strongly encourage code deposition in a community repository (e.g. GitHub). See the Nature Research [guidelines for submitting code & software](#) for further information.

Data

Policy information about [availability of data](#)

All manuscripts must include a [data availability statement](#). This statement should provide the following information, where applicable:

- Accession codes, unique identifiers, or web links for publicly available datasets
- A list of figures that have associated raw data
- A description of any restrictions on data availability

Coordinates and structure factors were deposited at the Protein Data Bank (PDB) under the accession codes 6FPF, 6FPG, 6HJW and 6H3P for Cmu1, the Cmu1/ZmKwl1 complex, ZmCm1 and ZmCm2, respectively.

The following figures have associated raw data: Extended Data figures 6, 9 and 12

The data that support the findings of this study are available from the corresponding authors upon reasonable request.

Field-specific reporting

Please select the best fit for your research. If you are not sure, read the appropriate sections before making your selection.

Life sciences Behavioural & social sciences Ecological, evolutionary & environmental sciences

For a reference copy of the document with all sections, see nature.com/authors/policies/ReportingSummary-flat.pdf

Life sciences study design

All studies must disclose on these points even when the disclosure is negative.

Sample size	No statistical methods were used to predetermine sample sizes. The sample size in the plant infection experiment (Fig. 1E) was based on previous studies in <i>Ustilago maydis</i> , where usually three biologically independent experiments, each with approximately 40 plants, were scored to evaluate the disease development. In this study we scored about 60 plants for each independent experiment.
Data exclusions	No data were excluded from the study.
Replication	All experiments were repeated independently and showed similar results. Number of repeats is given in the figure legends
Randomization	No randomization was required.
Blinding	No blinding was required.

Reporting for specific materials, systems and methods

Materials & experimental systems

n/a	Involvement in the study
<input type="checkbox"/>	<input checked="" type="checkbox"/> Unique biological materials
<input type="checkbox"/>	<input checked="" type="checkbox"/> Antibodies
<input checked="" type="checkbox"/>	<input type="checkbox"/> Eukaryotic cell lines
<input checked="" type="checkbox"/>	<input type="checkbox"/> Palaeontology
<input checked="" type="checkbox"/>	<input type="checkbox"/> Animals and other organisms
<input checked="" type="checkbox"/>	<input type="checkbox"/> Human research participants

Methods

n/a	Involvement in the study
<input checked="" type="checkbox"/>	<input type="checkbox"/> ChIP-seq
<input checked="" type="checkbox"/>	<input type="checkbox"/> Flow cytometry
<input checked="" type="checkbox"/>	<input type="checkbox"/> MRI-based neuroimaging

Unique biological materials

Policy information about [availability of materials](#)

Obtaining unique materials

Antibodies

Antibodies used

Validation

Validations of all primary antibodies are available on the manufacturer's websites: Anti-HA (<https://www.sigmaaldrich.com/catalog/product/sigma/h6908?lang=de®ion=DE>), Anti-His (<https://www.qiagen.com/de/shop/sample-technologies/protein/expression-purification-detection/penta-his-hrp-conjugate-kit/#orderinginformation>).